0 0 0 0 4 2 0 7 4 9 8

LBL-3172
c.1

COMPUTER SIMULATION OF SPUTTERING

Pravin Vasudeva Mundkur
(M. S. thesis)

RECEIVED
LAWRENCE
RADIATION LABORATORY

FEB 20 1975

LIBRARY AND
DOCUMENTS SECTION

December, 1974

Prepared for the U. S. Atomic Energy Commission
under Contract W-7405-ENG-48

For Reference

Not to be taken from this room

LAWRENCE BERKELEY LABORATORY
UNIVERSITY OF CALIFORNIA
BERKELEY

LBL-3172
c.1

DISCLAIMER

This document was prepared as an account of work sponsored by the United States Government. While this document is believed to contain correct information, neither the United States Government nor any agency thereof, nor the Regents of the University of California, nor any of their employees, makes any warranty, express or implied, or assumes any legal responsibility for the accuracy, completeness, or usefulness of any information, apparatus, product, or process disclosed, or represents that its use would not infringe privately owned rights. Reference herein to any specific commercial product, process, or service by its trade name, trademark, manufacturer, or otherwise, does not necessarily constitute or imply its endorsement, recommendation, or favoring by the United States Government or any agency thereof, or the Regents of the University of California. The views and opinions of authors expressed herein do not necessarily state or reflect those of the United States Government or any agency thereof or the Regents of the University of California.

0 0 0 0 4 2 0 1 4 9 9

Table of Contents

ABSTRACT v

PART I: SPUTTERING RATIO DEPENDENCE ON PARAMETERS OF THE POTENTIAL FUNCTION DESCRIBING ION-TARGET INTERACTIONS . . 1

ABSTRACT 1

I. INTRODUCTION 2

A. Dependence of the Sputtering Ratio on Potential Function Parameters 3

1. The Potential Function 3

2. Binding Energy 4

3. Experimental Data 4

4. Extrapolation of Data for Sputtering of Copper by Neon 5

5. Search for Suitable Potential Functions 12

a. Prediction from available theories 12

b. Simulation results: relationship between potential function and sputtering ratio 18

6. Correlation Between the Parameters of the Potential Function and The Sputtering Ratio 22

7. Discussion 34

B. Determination of the Potential Function Parameters from Sputtering Ratio Data for Mono-crystalline Target 36

1. Introduction 36

2. Analysis of the Problem 36

3. Procedure for Calculations 39

4. Results 39

5. Discussion 43

6. Effect of Entrapped Ions 49

7. Conclusion 52

REFERENCES 53

SYMBOLS 55

PART II: COMPUTER SIMULATION OF OBLIQUE INCIDENCE SPUTTING OF (100) Cu BY Ne^+ 59

ABSTRACT 59

1. Introduction 60

2. Summary of Relevant Experimental Results from the Literature 62

3. Theory 67

4. Simulation Method and Procedure 70

5. Potential Function 70

6. Simulation Results and Discussion 71

7. Conclusion 77

REFERENCES 78

LIST OF SYMBOLS 79

APPENDIX (The Simulation Model) 80

1. General Description 80

2. The Potential Function 81

3. Choice of Numerical Integration Procedure 83

4. Energy Decrement 86

5. Computation of $\langle F_i \rangle$ 86

6. Choice of Δt 87

7. Designation of Sputtered Atoms 88

8. Representative Areas 88

REFERENCES 92

LIST OF SYMBOLS 93

0 0 0 0 4 2 0 1 5 0 0

COMPUTER SIMULATION OF SPUTTERING

Pravin Vasudeva Mundkur

Inorganic Materials Research Division, Lawrence Berkeley Laboratory and
Department of Chemical Engineering; University of California
Berkeley, California

ABSTRACT

Part I:

The dependence of the sputtering ratio on the potential function describing the interactions between an incident neon ion and copper target atoms was studied with the help of a computer simulation model of sputtering. The results of this simulation indicate that the variation of the sputtering ratio with incident ion energy is dominated by the nature of the Ne^+-Cu interatomic potential function. The results of the simulation correlate well with prediction of the simple theory put forward by Magnuson.

Data on the sputtering of single crystal copper was used to extract information about the potential function for Cu-Cu interactions in the energy regions over which the sputtering data was available. The Ne^+-Cu and Cu-Cu interaction potentials were so derived that the variation of the sputtering ratio for the three Cu crystal faces (111), (100) and (110) matched experimental data. In addition, the Cu-Cu interatomic potential was adjusted so that repulsive force contributions matched the experimental elastic moduli of copper. The derived potentials differed significantly from the Gibson-2 potential which

had been used for Cu-Cu interactions in all previous sputter simulations. The above method for backing out information on interatomic potentials could prove useful in obtaining information on potential functions at energies where information has thus far been lacking.

Part II:

A computer simulation model was applied to calculate the sputter ratio of (100) Cu by 10 keV Ne^+ ions at incidence angles from 20° to 50° from the surface normal in the (110) plane. The calculation results show maxima and minima in the sputter ratio at incident angles in relative agreement with the experimental data of Onderdelinden. A submaximum in sputter yield was obtained near the 45° minimum. The peak was larger for Ne^+ sputtering than for Ar^+ sputtering of copper.

0 0 0 0 4 2 0 1 5 0 1

PART I: SPUTTERING RATIO DEPENDENCE ON PARAMETERS OF THE POTENTIAL FUNCTION DESCRIBING ION-TARGET INTERACTIONS

ABSTRACT

Normal incidence sputtering of (100) and (111) Cu by Ne^+ was investigated with a computer simulation model. The dependence of the sputtering ratio on the incident ion energy and on the parameters of the ion-target potential function were studied. The results show that sputtering on the (hkl) face can be simply described by an extension of a theory by Magnuson.

A calculated sputter ratio equation was used to estimate the magnitude of the Cu-Cu interatomic potential function at interatomic separations between 0.1 and 1 times the equilibrium nearest neighbor distances.

I. INTRODUCTION

The potential energy function which describes the interactions between the incident ion and the target atoms will govern the pattern of transfer of kinetic energy during sputtering. Hence, the sputtering ratio--the number of target atoms sputtered per incident ion--can be expected to depend on this potential energy function in some fashion.

Computer simulation provides a convenient method for studying this dependence, since the potential function can be independently varied over a wide range, while all other properties that affect the sputtering ratio are kept constant. The high degree of controllability and observability offered by numerical simulation is not readily available to the experimentalist.

Simulation of the sputtering of monocrystalline target allows comparison with accurate experimental data. The sputtering ratio of polycrystalline targets, on the other hand, depends very much on the proportion of the various oriented crystallite faces present on the surface, leading to significant discrepancies in the data of different authors. Data on the sputtering of monocrystals is not subject to such uncertainties.

Harrison et al.[1-4] have developed a computer simulation model to simulate the sputtering of a monocrystalline F.C.C. metal by rare-gas atoms. The model is described in detail in the Appendix. This computer model was used in this study to simulate the sputtering of monocrystalline copper by Neon, from which a potential function suitable for describing Neon-Copper interactions was derived. The variation of the sputtering

ratio with parameters of the potential function was also studied. From the simulation results a relationship between the sputtering ratio and the potential function parameters and incident ion energy was derived. Finally, in section B, the results of section A are applied to outline a method for deriving potential functions from data on the self sputtering of single crystals. The method is applied to data on the sputtering of monocrystalline copper by Cu^+ ions to derive two slightly differing potentials to describe the Cu-Cu interactions. These potentials are compared with potentials which have been cited in the literature to represent Cu-Cu interactions.

A. Dependence of the Sputtering Ratio on Potential Function Parameters

1. The Potential Function

In order to calculate the forces exerted between atoms it is necessary to have a potential function describing the interactions between these atoms. The interactions between atoms may be represented by a Born-Mayer type potential function.

$$V(r) = \exp\,(P_A + P_B \cdot r) \tag{1.1}$$

where, V(r) is the interatomic potential energy in eV, P_A, P_B are the parameters of the potential function, and r is the distance between the atoms.

An equivalent form of Eq. (1.1) is

$$V(r) = E_o \exp(P_B \cdot r) \tag{1.2}$$

where

$$E_o = \exp\ (P_A) \tag{1.3}$$

The form of Eq. (1.1) is used in the present work since it is more suitable for computer calculation. The unit of distance is the lattice unit (l.u.), defined as half the unit cell lattice parameter for copper, i.e., 1 l.u. = 1.8075Å.

The interactions between copper atoms can be described by the Gibson-2 (GB-2) potential, which has been used in previous computer simulation models.[1,5,23] This potential function was estimated by Huntington et al.[6,7] from work on point defects and self-diffusion in F.C.C. metals. The parameters of this function are given in Table 6. In this study, the parameters of the potential function describing interactions between the Neon and copper atoms were varied over a wide range. The pattern of variation of the sputtering ratio was then studied with respect to this variation.

2. Binding Energy

A binding energy must be specified in the computer model in order to estimate sputtering ratio. This specification is described in the Appendix. In accordance with previous work by Harrison[1-4] a binding energy of 2.4 eV was used in this study.

3. Experimental Data

Experimental data for the sputtering of poly-crystalline and mono-crystalline copper by Argon and Neon are available from several sources. Source literature on the sputtering of polycrystalline

copper is available from the comprehensive review by Carter et al.[8]

The sputtering of mono-crystalline copper by Argon has been investigated by Southern et al.[9] for the following incident ion energy range and crystal surface orientations: [1-5KeV, (110), (100), (111)]. Magnuson et al. studied the range [1-10 KeV, (110), (100), (111)] and the Amsterdam group[11,12] studied the range [20 KeV, (100), (111)].

Sputtering of mono-crystalline copper by Neon has been investigated by McKeown et al.[13] in the range [0.5 KeV, 1.0 KeV, (111)] and by the Amsterdam group[11,12] in the range [10 KeV, 20 KeV, (100), (111)]. In addition, Onderdelinden[14] has carried out experiments to obtain the sputtering ratios for Ar^+, Kr^+ and Cu^+ on Cu in the range [5-30 KeV, (110), (100), (111)] and Ar^+ on Au in the range [5-30 KeV, (100)].

4. Extrapolation of Data for Sputtering of Copper by Neon

The available data for the sputtering of copper by Neon are sparse. The data are summarized in Table 1. The point corresponding to 10 KeV ion energy for sputtering of the (100) face was obtained by extrapolation from the data of Elich et al.[12] These authors studied the variation of the sputtering ratio with the angle of 10 KeV Ne^+ ion. Unfortunately, they did not obtain data for normal ion incidence. Extrapolation of their data to normal incidence is possible, however. From the sputter ratio S at the (110) minimum angle Q (approximately 45° from the normal), and at normal incidence, we find

S_{Ne}((110) minimum, 10 KeV on (100)Cu) = 1.75 atoms/ion ,

S_{Ne}((110) minimum, 20 KeV on (100)Cu) = 1.4 atoms/ion , and

S_{Ne}(normal incidence, 20 KeV on (100)Cu) = 1.5 atoms/ion .[12]

Table 1. Experimental Sputter Ratios for Neon

Ion Energy (KeV)	Crystal Surface	
	(100)	(111)
20	1.5[12]	2.4[11]
10	1.87*	---
1.0	--	2.75[15]
1.5	--	2.1[13]

*See Text, page 7.

Hence, the sputter ratio S_{Ne} (at normal incidence, 10 KeV on (100)Cu)

$$\approx \frac{1.75}{1.4} \; 1.5 = 1.87 \text{ atoms/ion} .$$

It is possible to predict, approximately, the shape of the curve for the sputtering of mono-crystalline copper by Neon from the available data. The procedure used for prediction of the shape of the curve is illustrated below for the case of (111) copper since most of the work was done with this face. The (111) surface provides the most distinct maximum in the sputtering ratio as a function of ion energy (here referred to as the S-E curve). First we attempt to predict the location of the maximum in the S-E curve for (111) Cu and also the approximate magnitude of the sputtering ratio at this point.

As will be clarified below, the sputtering ratio of a monocrystal follows approximately the law

$$S \propto E_r^{1/2} \, r_c^{n} \quad , \tag{4.1}$$

where r_c is the hard sphere collision radius for an ion-target collision, the exponent n is approximately equal to 2 for a monocrystalline target. E_r is the incident ion energy in center-of-mass coordinates, given by:

$$E_r = \frac{M_2}{(M_1 + M_2)} \; E \tag{4.2}$$

where, E is the energy of the incident ion, M_1 is the incident ion mass, and M_2 is the target atom mass. If the interatomic potentials are of the Born-Mayer type, r_c is contained in the equation

$$E_r = V(r_c) = E_o \exp (P_B \cdot r_c) \ . \text{ --- (e.v.)}$$

Hence, solving for r_c, we obtain

$$r_c = \frac{\ln (E_o/E_r)}{(-P_B)} \quad \text{(l.u.)} \ . \tag{4.3}$$

Substituting Eq. (4.3) into Eq. (4.1) and differentiating with respect to E_r, we obtain a simple expression for the center-of-mass energy, E_r, max, at which the maximum sputtering ratio, S_{max} is obtained:

$$\ln (E_{r,max}) = \ln (E_o) - 2n = P_A - 2n \ .$$

The exponent n is generally not the same for monocrystalline and polycrystalline phases. Using the subscript m to denote a monocrystalline target, the subscript p to denote a polycrystalline target and subscripts 1 and 2 to identify two different incident ion types, we have

$$\ln (E_{r,max,1,p}) = P_{A1} - 2n_p$$
$$\ln (E_{r,max,2,p}) = P_{A2} - 2n_p$$
$$\ln (E_{r,max,1,m}) = P_{A1} - 2n_m$$
$$\ln (E_{r,max,2,m}) = P_{A2} - 2n_m$$

and hence,

$$\frac{\ln (E_{r,max,2,p})}{\ln (E_{r,max,1,p})} = \frac{P_{A2} - 2n_m}{P_{A1} - 2n_m} \tag{4.4}$$

if we assume that the difference $|n_p - n_m| \ll P_A - 2n_m$.

The relationship expressed by Eq. (4.4) was tested by using experimental data for the sputtering of Cu by Ar^+ and Kr^+ ions. The relevant data are summarized in Table 2. Using the subscript 2 for Kr and 1 for Ar, we have:

$$\frac{\ln (E_{r,max,1,m})}{\ln (E_{r,max,2,m})} = 1.128 \quad \text{and} \quad \frac{\ln (E_{r,max,1,p})}{\ln (E_{r,max,2,p})} = 1.176 \ .$$

These two ratios agree within 5%. Also, the sputter ratios are

$$\left[\frac{S_{max,(111)}}{S_{max,poly}}\right]_{Kr} = 1.08 \quad \text{and} \quad \left[\frac{S_{max,(111)}}{S_{max,poly}}\right]_{Ar} = 1.20 \ .$$

These two ratios agree within about 10%, with a mean of about 1.114. Hence, $S_{max,(111)} \propto 4.00 \pm 10\%$ (atoms/ion), and $\frac{\ln(E_{r,max,1,p})}{\ln(E_{r,max,2,p})} = 1.177$. Therefore we find $\ln(E_{r,max,2,(111)}) = 1.236 \pm 5\%$ and the energy at which the maximum occurs in the S-E curve for normal incidence on (111) copper by Neon is $E_{1,max,(111)} = 4.54 \pm 7\%$ (KeV). Similar calculations were performed for the (100) crystal face, and the results summarized in Table 3.

In the above table, M_1=Mass of the incident ion, M_2= Mass of the target, S_{max} = Maximum Sputtering ratio as a function of E, and E_{max} = Energy at which this maximum occurs.

Table 2. Sputtering of Cu by Ar and Kr at Normal Incidence.

Ion Type	Surface Type	E_{max} (Atoms/Ion)	E_{max} (KeV)	$\frac{M_2}{M_1}$	$\frac{M_2}{M_1+M_2}$	E_r (KeV)
Kr	Polycrystalline[15]	13.0	100.0	0.7582	0.4312	43.12
	(111)[13]	14.0	12.0			5.17
Ar	Polycrystalline[15]	7.5	40.0	1.5905	0.614	24.56
	(111)[13]	9.0	7.0			4.30

(a) Note: Polycrystalline sputtering curves are very dependent on the the proportion of the various crystal faces that are present on the polycrystalline surface. Care must be taken to obtain data from the same source, if comparative calculations, of the present nature, are to be made. The above values were taken from the data of Almén et al.,[15] and Dupp et al.[30]

Table 3. Predicted Sputtering Ratios of Neon Sputtering of Monocrystalline Copper[a]

Crystal Surface			
(111)		(100)	
Ion Energy	(atoms/ion)	Ion Energy	(atoms/ion)
0.5 KeV	2.1[13]	2.8±7%	(1.95±10%)
1.0 KeV	2.75[13]	5.0	(1.9)
4.5±7%	(4.0±10%)	10.0	(1.87)
10.0	(3.65)	20.0	1.5[12]
20.0	2.4[12]		

[a]Except for referenced values, all values are estimated by the method in the text. Referenced values are experimental. Estimated values are given in parentheses.

5. Search for Suitable Potential Functions

a. Prediction from available theories. Sputtering by ions in the energy range from approximately 1 keV to 20 keV was studied as a function of interatomic potential function parameters in order to predict sputter rates for conditions where there is no accurate data. An attempt was made to predict the parameters of the potential functions in accordance with the recommendations of several authors.

Abrahamson[17] has provided a table of Born-Mayer potential parameters for interactions between like atoms, with atomic numbers varying Z=2 to 105. For unlike atoms he recommended the use of a root-mean potential. For example, if A-A interactions are given by:

$$V_A(r) = E_A \exp(P_{B_A} \cdot r)$$

and B-B interactions by:

$$V_B(r) = E_B \exp(P_{B_A} \cdot r)$$

then, A-B interactions may be represented by:

$$V_{AB}(r) = E_{AB} \exp(P_{B_{AB}} \cdot r)$$

where

$$E_{AB} = \sqrt{E_A \cdot E_B}$$

and

$$P_{B_{AB}} = (P_{B_A} + P_{B_B})/2.0 \ .$$

The parameter values $P_A=\ln(E_A)$ and P_B obtained in accordance with these recommendations are summarized, for several interactions, in Table 4.

As a check on the recommended interatomic potential function for Cu, equations given by Huntington[18] were used to calculate the contribution of the repulsive forces to the elastic module of copper. This contribution may be estimated from the following equations:

$$C_{11} = \sqrt{2} \cdot r_o^{-1} V''(r_o) + r_o^{-1} V'(r_o) \tag{5.1}$$

$$C_{12} = \frac{1}{\sqrt{2}} \cdot r_o^{-1} V''(r_o) - 5r_o^{-1}V'(r_o) \tag{5.2}$$

$$C_{44} = \frac{1}{\sqrt{2}} \cdot r_o^{-1} V''(r_o) + 3r_o^{-1}V'(r_o) \tag{5.3}$$

$$B = (C_{11} + C_{12})/3.0 \; . \; . \; . \tag{5.4}$$

where, C_{11}, C_{12}, C_{44} are the elastic moduli of copper, B is the Bulk Modulus of Copper, r_o is the nearest neighbor distance and $V'(r_o)$ and $V''(r_o)$ denote first and second derivatives of V(r) evaluated at $r=r_o$. For copper, r_o=2.551Å. A summary of the results of the calculations, using these equations, is shown in Table 5.

The values listed for GB-2 are in reasonably good agreement with experiment.[19] However the potential recommended by Abrahamson (AB-Cu) gives values that are off by an order of magnitude. We may conclude that this potential is much too strong at atom separations around the nearest neighbor distance. In the simulation, the GB-2 potential was used throughout to represent interactions between copper atoms.

Table 4. Born-Mayer parameters by Abrahamsons recommendations

Atom Interactions	$P_A = \ln E_A$	P_B, $(l.u.)^{-1}$
Ne-Ne	8.046	- 6.830
Ar-Ar	8.848	- 6.555
Cu-Cu[a]	9.541	- 6.437
Cu-Cu[b]	10.0241	- 9.1967
Ar-Cu[c]	9.436	- 7.876
Ne-Cu[c]	8.7935	- 6.6335

(a) Abrahamson's recommended values
(b) Gibson-2 (GB-2) potential for copper.[5]
(c) Based on Abrahamsons recommendations for the Cu-Cu potential

Table 5. Elastic Module of Copper (Units: 10^{11} dynes/cm^2) from equations (4.6-1) to (4.6-4)[a]

Potential used	C_{11}	C_{12}	C_{44}	B
GB-2	10.9	8.1	4.5	9.0
AB-Cu	155.0	135.1	58.3	141.7
P_{Cu}-1	11.0	7.7	4.8	8.8
P_{Cu}-2	10.9	7.7	4.7	8.8
Experiment[20] (0°K)	17.6	12.5	8.2	14.2

[a] Contribution of the interactions of the conduction electrons with ion cores[5] is about 5.0×10^{11} dynes/cm^2 for C_{11}, C_{12} and B and 2.6×10^{11} dynes/cm^2 for C_{44}. These numbers must be added to the corresponding calculated figures in the above table before a comparison is made with the experimental values listed there.

Some of the potentials recommended by Abrahamson for the Ne-Cu interactions (AB-Ne-Cu) and for Ar-Cu interactions* (AB-Ar-Cu), were used in the simulation. Results of the study indicate that the sputtering ratios obtained by the computer simulation are too low as compared to experimental values (for Argon) and to values extrapolated from experimental data (for Neon). The results are summarized in Table 6.

Anderson et al.[20] recommended the semi-empirical relation $V(r) = A_o e^{(-r/a_A)}$ with $A_o = 52\ (A_1 Z_2)^{3/4}$ e.v. and $a_A = 0.219$Å. This model gives, $P_A = 8.203$ for Neon-Copper and $P_A = 8.618$ for Argon-Copper interactions with $P_B = -8.253$ for both.

These functions were found to be too soft to use for sputtering ratio predictions and were not used in the simulation. The Born-Mayer approximations to the Harrison-Wedepole potentials for Ne-Cu and Ar-Cu interactions (HW-Ne-Cu; WH-Ar-Cu) were also found to give very low sputtering ratios.

Previous work on ion-range distributions[23] and sputtering ratios[10] has provided evidence that the Bohr interatomic potential[21] is not valid in the energy range of interest. This potential function is given by:

$$V(r) = \frac{Z_1 Z_2 \ell^2}{r \pi \varepsilon_o r} \exp(-r/a_B) \qquad (5.5)$$

*Professor D.E. Harrison, Jr., (Private Communication)

Table 6. Simulation values for the sputtering of Copper by Neon.

Potential Function			Lattice Surface	Sputtering Ratio at Normal Incidence (Atoms/Ion)				N_{oo} of Impart Points
Function used	P_A	P_B		0.5 keV	1.0 keV	5.0 keV	10.0 keV	
HW-Ar-Cu	8.48	- 6.28				1.40		
HW-Ne-Cu	8.67	- 7.64				0.91		
KSE-B	11.1747	- 8.301				6.82		
AB-Ne-Cu	8.794	- 6.634	(100)			1.37		
V1	9.00	- 6.67				1.74		
V2	9.25	- 6.87			3.28	1.74		(35)
V3	9.25	- 7.57			3.12			
V4	9.25	- 8.301			2.06			
V5	9.50	- 8.301			2.94			
V6	9.47	- 8.301		2.46			1.14	
					2.3	1.45	1.5	
V7	10.5	- 9.36	(111)		3.35	2.05	2.15	
V8	11.5	-10.9			3.25	3.2	3.45	(20)
V9	12.5	-12.71			2.9	4.3	3.45	
Extrapolated	from	Experiment	(100)			1.9	1.87	
			(111)	2.1	2.75	4.0	3.65	

0 0 0 0 4 2 0 1 5 0 8

In the energy range from 1 eV to 40 keV, Eq. (5.5) gives much too low and energy of interaction when used in sputtering simulations. Hard core cross-sections of four to six times the ones predicted by Eq. (5.5) must be used in order to explain the experimental data.[10,23]

Firsov[24] modified the above potential function to obtain $a_F = 0.8854\ a_o(Z_1^{1/2} + Z_2^{1/2})^{-2/3}$ instead of a_B in Eq. (5.5) Lindhard et al.[25] recommended the alternate $a_L = 0.8853\ a_o(Z_1^{2/3} + Z_2^{2/3})^{-1/2}$. Neither of these recommendations, however, alters the potential function substantially. The Thomas-Fermi-Diroi expressions of Gombes[26] cannot be used for separations greater than about 1.0Å.[5]

b. Simulation Results: relationship between potential function and sputtering ratio. In the absence of any literature data for deducing the required potential functions, a number of trial functions were used in the simulation. These trials were followed by a more systematic variation of the potential function until a better agreement with the experimental data was obtained.

In Fig. 1 is shown a plot of two potential functions on a semi-log scale. For an incident ion energy E_o, most of the collisions in the first few atomic layers will take place at energies in the range ΔE. These are the collisions of importance for the sputtering phenomenon.

Hence, if V_1 and V_2 do not differ excessively from each other and if they cross at some point within this region ΔE we would expect that the mean energy and cross-sections of the atom-atom interactions would be approximately the same. We can then conclude that the sputtering ratio at energy E_o would be approximately the same for both functions V_1 and V_2.

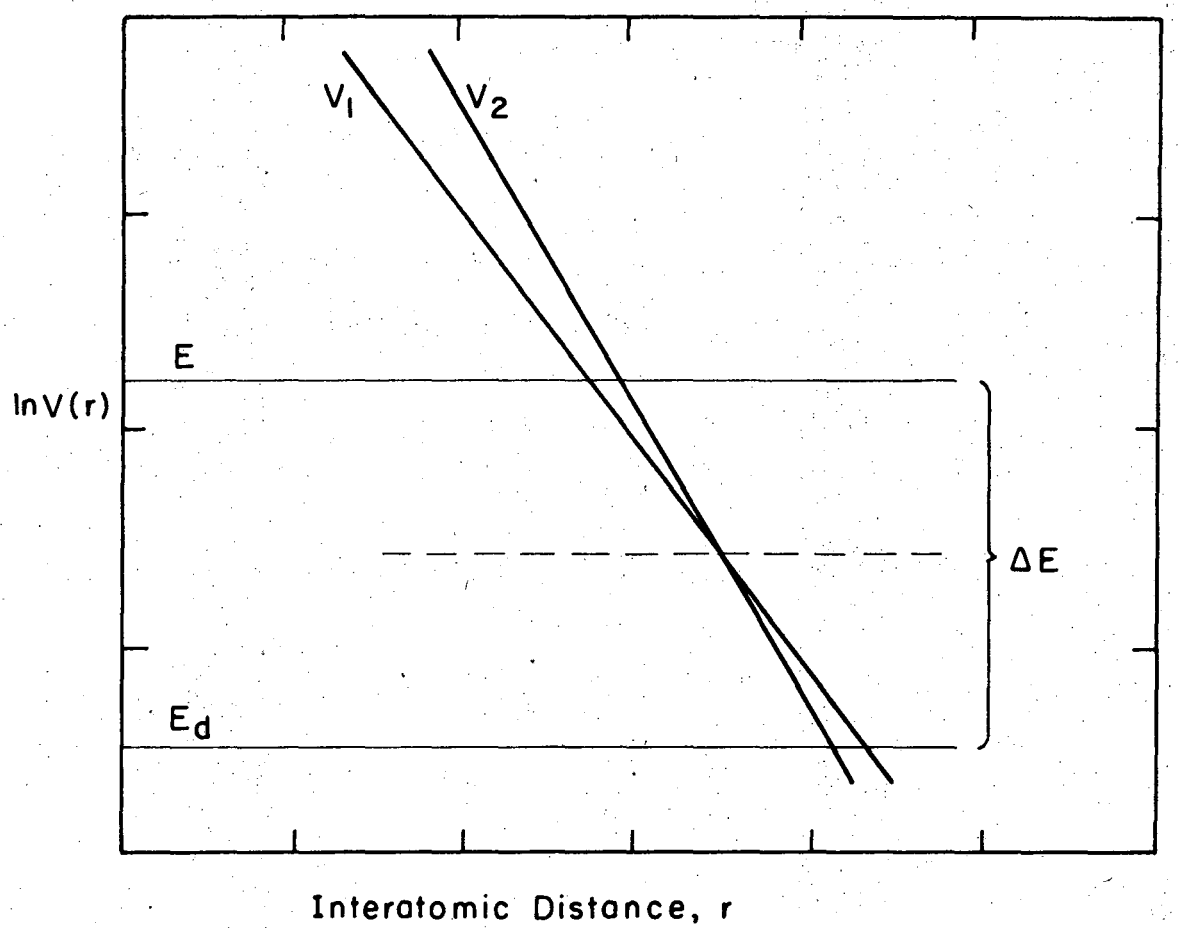

$V_1 = \mathrm{Exp}\,(P_{A_1} + P_{B_1 r})$

$V_2 = \mathrm{Exp}\,(P_{A_2} + P_{B_2 r})$

E_d = Displacement energy for copper

E = Incident ion energy

XBL 7412-7654

Fig. 1. Potential energy of interaction of two atoms versus the distance between the two atoms, for two different potentials P_1 and P_2.

At ion energies significantly higher than E_o the effective hard sphere radii of the atoms can be seen to be greater on the average for V_2. Hence the probability of collisions is higher, and we should obtain a higher sputtering ratio with the use of V_2 than with V_1. At ion energies lower than E_o the reverse holds true and V_2 gives a smaller sputtering ratio than V_1.

Using the results of the above argument then, we first varied one parameter of the potential function until a fit to the experimental data was obtained at one end of the energy range of interest. This was termed the Match Point. Both parameters were then varied in such a fashion as to keep the sputtering ratios at the Match Point constant while varying the shape of the S-E curve over the total energy range. The computed S-E curves were then compared with the S-E curve predicted from experimental data.

The results of the simulation for four different potential functions V_6, V_7, V_8 and V_9 are shown in Fig. (2). The simulation points were obtained with a set of 20 impact points (see appendix), whereas in other simulation runs 35 impact points were used. Statistical variations were found to be considerable in the simulation results for 20 and 35 impact points, as is evidenced by the differences in the curves for the V_6 potential. But the general trend of the curves remained the same and gave a good indication of the validity of the assumed potential function.

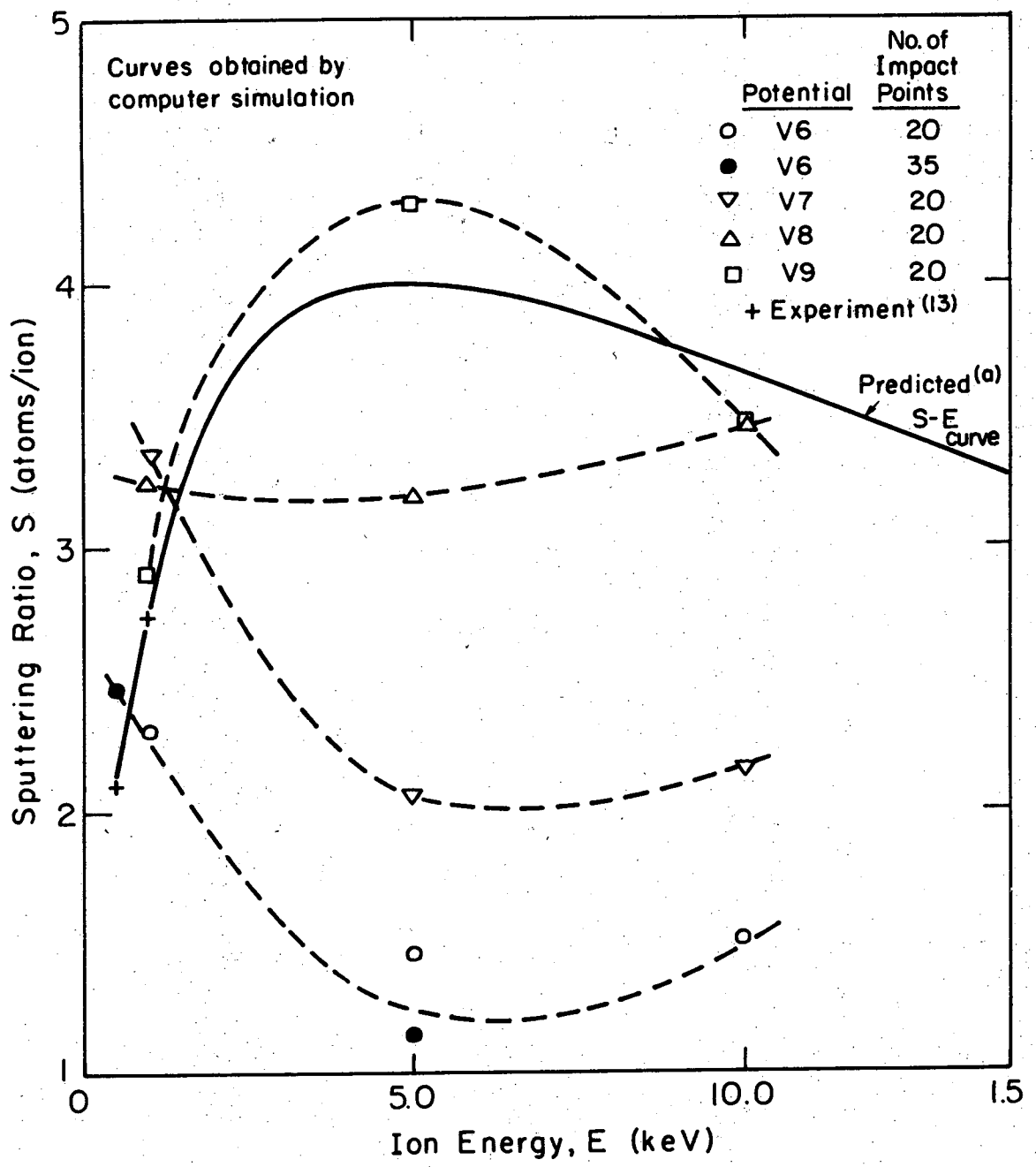

XBL 7412-7655

Fig. 2. Simulated sputtering ratio for Ne^+ on (111) copper for four different Ne-Cu potential functions. A graph of the experimental values, and values extrapolated from experiment, is provided for comparison.

The potential function V_6 was first established by successive trials so as to give agreement with experimental data at 1 keV. Potentials V_7, V_8, V_9 were then obtained successively, each as an improvement on the previous one, so as to maintain the sputtering ratio at 1 keV approximately at the experimental values, while changing the shape of the S-E curve till desired trends were obtained. The function V_9 gave a S-E curve which agrees reasonably with the predicted S-E curve to within the accuracy of the simulation method. Hence V_9 was used to represent Ne-Cu interactions in subsequent simulation studies, to be discussed in Section B, Part I of this thesis. A summary of the results of the various simulation runs for Neon-Copper sputtering is given in Table 6.

6. Correlation Between the Parameters of the Potential Function and the Sputtering Ratio

The intensity of the atom-atom interactions, leading to sputtering is largely governed by the energy of the incident ion. The probability of collisions is proportional to the effective cross section for collision of the atoms. The distance of closest approach for a given ion energy is a good measure of the apparent size of the atoms as they appear to each other at the time of collision. Hence if as before:

$$V(r) = E_o \exp (P_B \cdot r) \tag{6.1}$$

and

$$E_r = [M_2/(M_1+M_2)]\, E_o \tag{6.2}$$

the apparent hard-sphere collision radius is given by:

$$r_c = \frac{\ln (E_o/E_r)}{(-P_B)} \tag{6.3}$$

Here we assume that the incident ion is a point mass and that the effective collision radius is that of the target atom.

The sputtering ratio S, should depend on the intensity of the atom-atom interactions as well as the probability of these interactions. It would also depend on numerous other factors such as the relative masses of the incident ion and the target atom, the binding energy of the target atoms and the crystal structure of the target atoms. If, however, we restrict ourselves to the variation of S with E and r_c only, we may write

$$S = f(E,r_c) \tag{6.4}$$

where 'f' is some function of the crystal structure and the Miller indices of the surface.

Figure 3 shows the sputtering ratio obtained by the simulation, plotted against the hard sphere radius, r_c. The figure gives some evidence that S increases monotonically with r_c.

To obtain a more quantitative relation indicating, clearly, the trend for variation of S with E and r_c a number of other relationships between these variables were investigated, in the form $S=f(E^n r_c^m)$ where n=1/2,1 and m=1,2. The relation $S=f(Er_c^2)$ shown in Fig. 4 indicates that no general correlation exists between S and Er_c^2, which is valid at all ion energies studied. In contrast to the correlation of

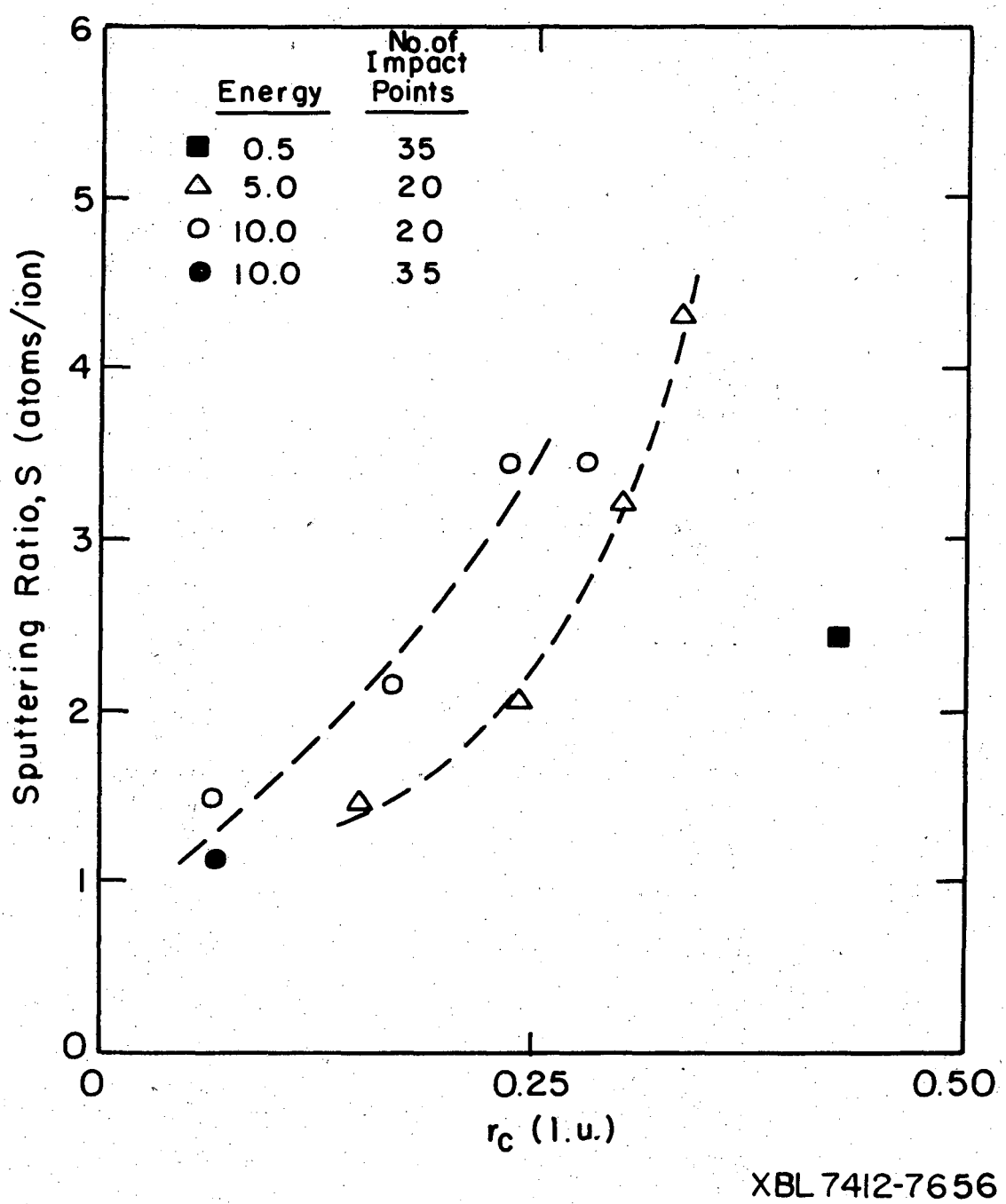

Fig. 3. Simulated sputtering ratios for Ne^+ on (111) copper, S(111), plotted against the hard sphere radii, r_c.

Fig. 4, Fig. 5, shows a plot of S vs $E^{1/2}\ r_c^{\ 2}$, and indicates a definite linear variation of S with $E^{1/2}\ r_c^{\ 2}$. The scatter of the points is large, possibly due to the fact that the number of impact points used for most of the points was low.

The linear variation of S with $E^{1/2}\ r_c^{\ 2}$ correlates well with a semi-empirical theory put forward by Magnuson et al.[10] to explain their experimental results on the sputtering of single-crystal copper and silver by Argon. In their model, Magnuson et al.[10] propose the following relation:

$$S(hkl) = K\ (hkl)\ E^{1/2}\ P_c\ (hkl) \qquad (6.5)$$

where, S(hkl) is the sputtering ratio for an ion incident on the (hkl) face of the crystal, K(hkl) is a constant depending on the crystal face (hkl) and on mass-dependent terms, P_c(hkl) is the probability that the incident ion makes a collision in the first few layers of the crystal, and E is the incident ion energy. Magnuson et al evaluated P_c for four different faces by assuming different hard sphere radii for the target atoms and by projecting all the atoms onto the front surface of the crystal. They thus computed the fraction of the total area that consisted of the projections from atoms that are exposed to impacts with the incident ion. Calculations were then performed utilizing a computer. The incident ion was assumed to be point mass.

Figure 6 gives a plot of the values of P_c(hkl) vs (r/a), reproduced from Magnuson et al.[10] In this plot r is the hard sphere radius of the target atoms with the incident ion visualized as a point mass, and a is the lattice constant of the target atoms.

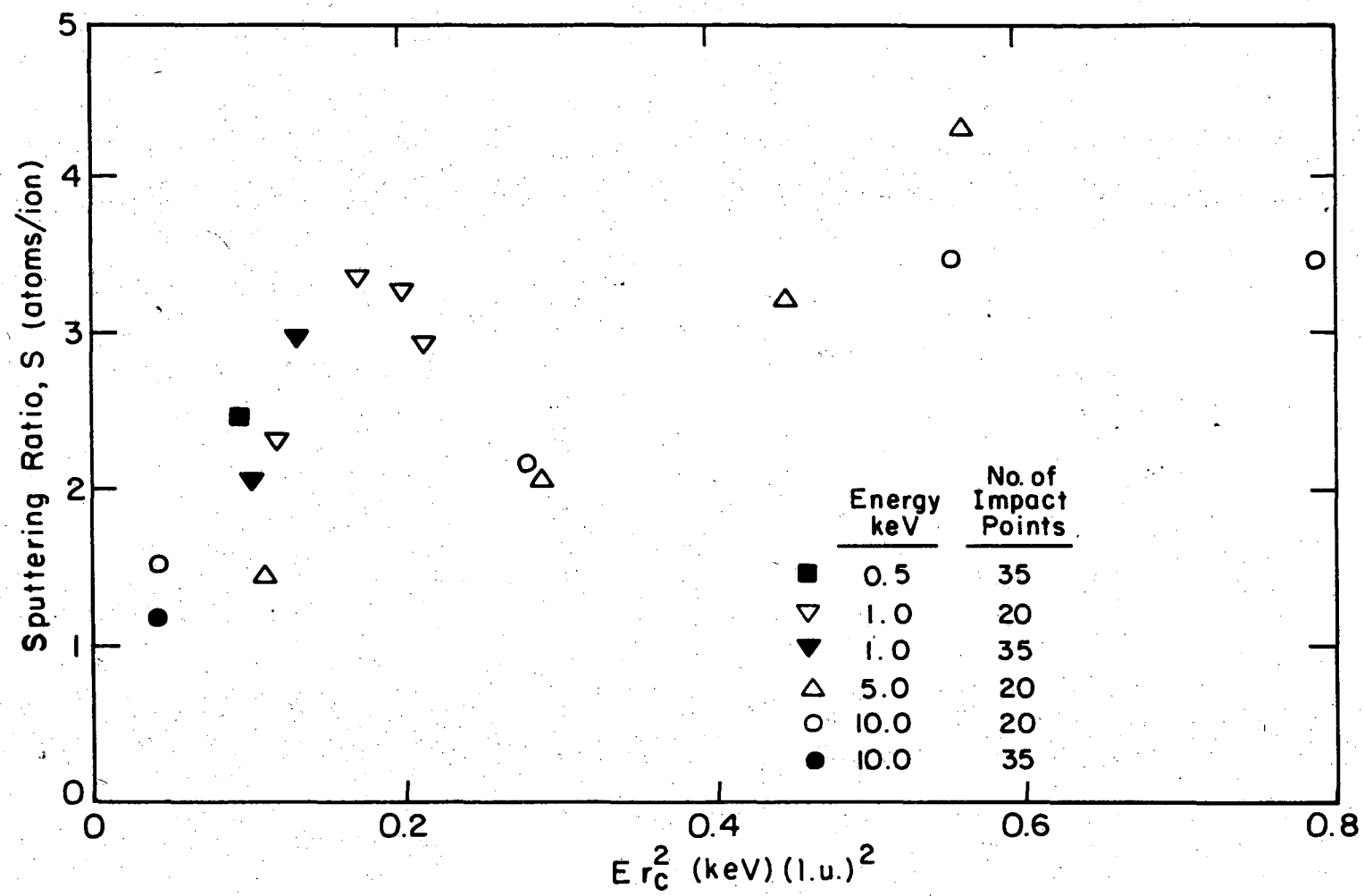

XBL 7412-7657

Fig. 4. Simulated sputtering ratios for Ne^+ on (111) copper, S(111), versus Er_c^2.

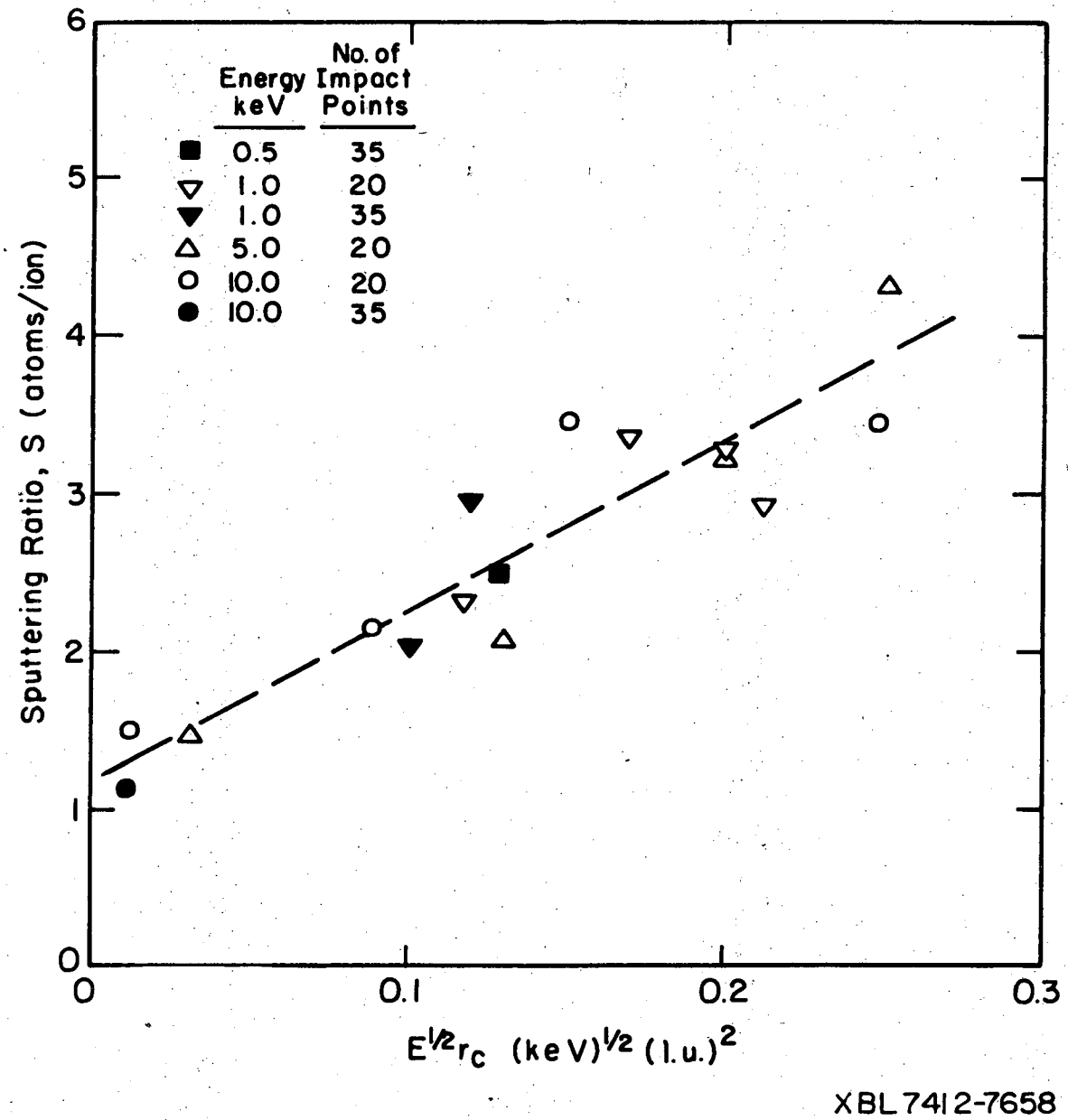

Fig. 5. Simulated sputtering ratios of Ne^+ on (111) copper, S(111), versus $E^{1/2} r_c^{\ 2}$.

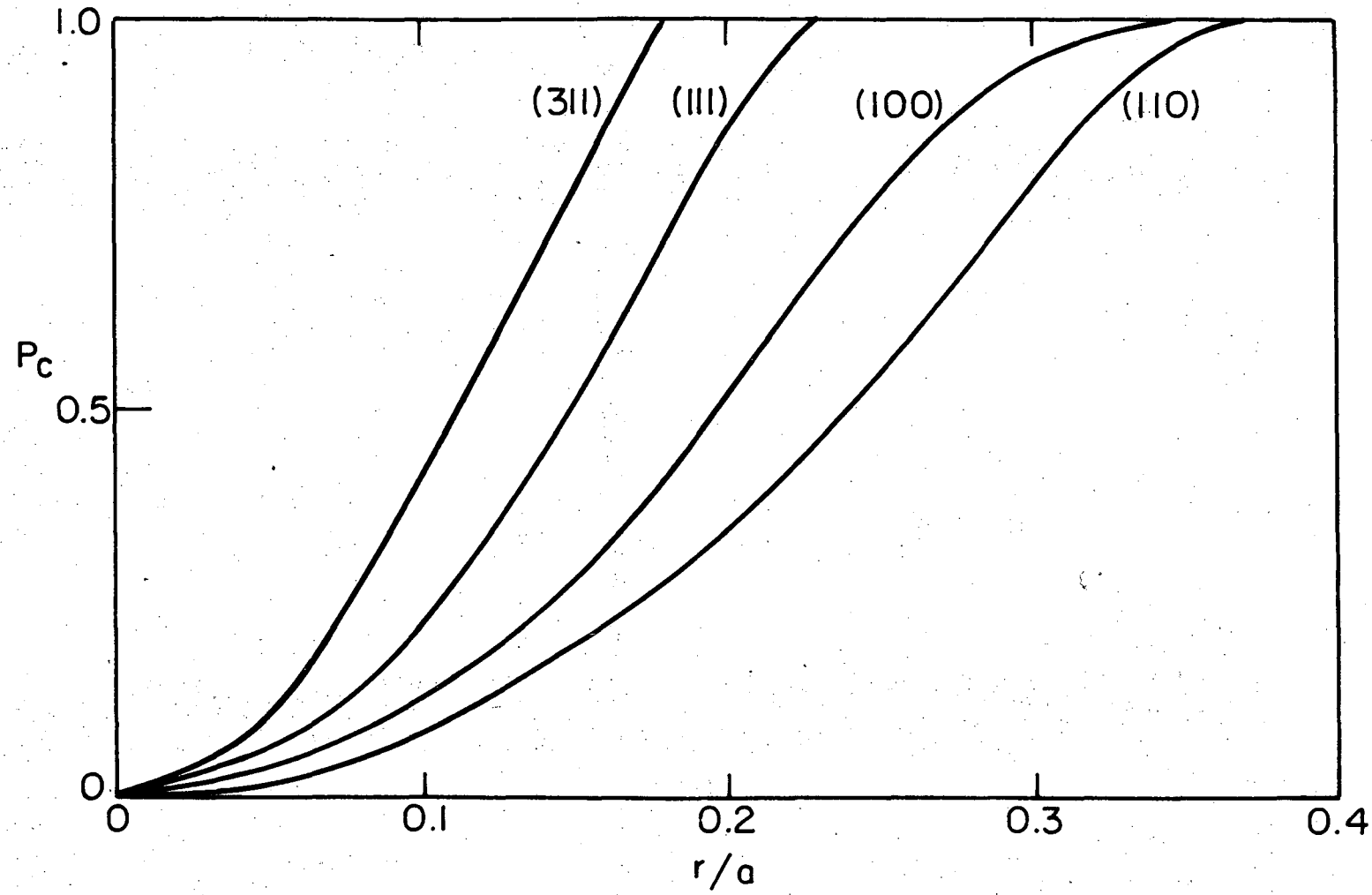

XBL 7412-7659

Fig. 6. Probability of ion-atom collisions P_c(hkl) plotted against 'reduced' hard sphere radii of atoms (r/a). Graphs for four different crystal orientations are presented.

To explore the variation of P_c with (r/a) more clearly, the data of Fig. 6 was replotted in a log-log plot of P_c vs (r/a) as shown in Fig. 7. This figure indicates linear dependence over a large range of (r/a) and suggests a simpler relationship between the variables of the form

$$P_c(hkl) = C(hkl)\ (r/a)^{n(hkl)} \tag{6.6}$$

where C(hkl) and n(hkl) are constants, dependent only on the surface orientation. The slopes of the functions in Fig. 7 were computed to be:

$$\begin{aligned} n(111) &= 1.95 \\ n(100) &= 1.925 \\ n(110) &= 1.900 \end{aligned} \tag{6.7}$$

These values are within 3% of each other, and hence, we obtain:

$$P_c(hkl) = C(hkl)\ (r/a)^{n} \tag{6.8}$$

where $n \simeq 1.925 \pm .025$. Magnuson et al., assumed a Bohr potential to represent interactions between incident ions and target atoms,

$$V(r) = (Z_1 Z_2 \ell^2/r)\ \exp(-r/a_B) \tag{6.9}$$

where

$$a_B = k\ a_o\ (Z_1^{2/3} + Z_2^{2/3})^{-1/2}$$

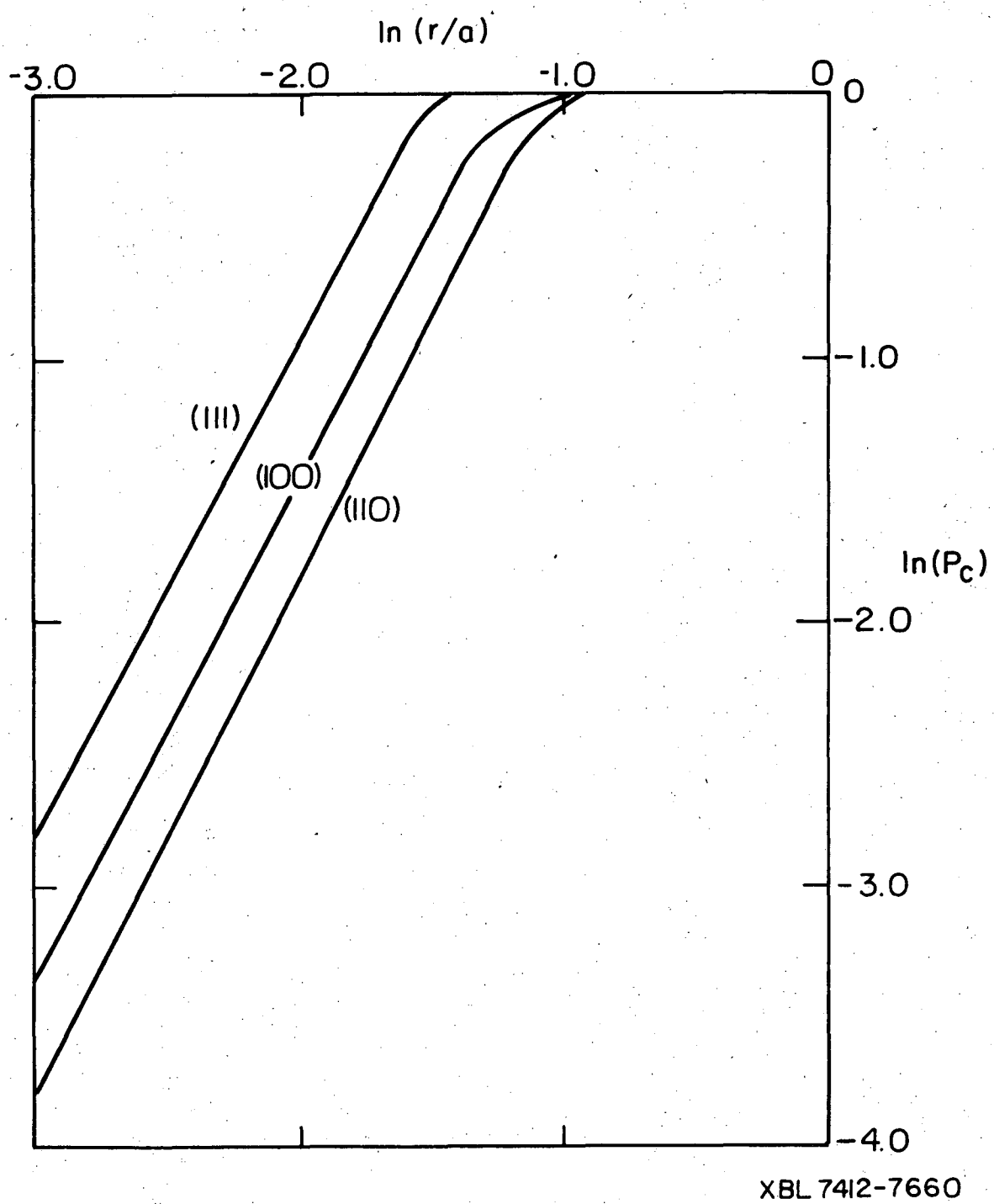

Fig. 7. Plot of ln P_C(hkl) versus ln (r/a) for four different crystal orientations.

and k is an adjustable parameter. The hard core radius was estimated by using Eq. (6.9) for the interatomic potential. However, the cross-section thus obtained did not give a large enough cross-section to obtain a fit with the experimental data and Magnuson et al. were forced to assume in the calculations that

$$R = C\, R_{H \cdot C} \tag{6.10}$$

where, $R_{H \cdot C}$ is the hard core radius estimated with the Bohr potential of Eq. (6.9), C is an adjustable constant and R is the radius used with the curves to determine P_c. With these adjustable parameters Magnuson et al. were able to obtain a good fit to their experimental data. The values they assumed in order to obtain this fit are indicated in Table 7.

Table 7. Values of adjustable parameters used by Magnuson et al.[10] to obtain a fit with their experimental data.

Metal \ Constant	K(111)	K(100)	K(110)	k	c
Cu	4.60	3.45	3.20	1.20±0.20	2.35±0.05
Ag	5.40	4.50	3.90	1.50±0.20	2.45±0.05

In order to illustrate the agreement between the results of Magnuson et al. and our simulation, a plot of the simulation sputtering ratio versus $E^{1/2}P_c(111)$ was made. For determination of P_c values, r_c was first calculated using Eqs. (4.3) and (4.2), for each potential function and ion energy. These values of r_c were then used with Fig. 7 to determine the corresponding values of P_c. The dependence of S vs $E^{1/2}P_c$ is shown in Fig. 8.

By comparison with Fig. 5 it can be seen that the statistical scatter is considerably diminished and that the linear variation of S with $E^{1/2}P_c(111)$ is clearly displayed. Hence, the simulation results can be summarized in the equation,

$$S(111) = S_o + K_1 E^{1/2} P_c(111) \tag{6.11}$$

where S_o and K_1 are constants, S_o = 1.9 atoms/ion, and K_1 = 2.8 atoms/(ion-keV$^{1/2}$).

The fact that S_o is non zero could be caused by any of the following:

(i) We used only a small set of impact points in our simulation. With the use of a small set of impact points,[20] it was difficult to obtain a statistically uniform distribution of points over the representative area (see Appendix A). This introduces a systematic error into the simulation results.

(ii) Limitations are inherent in the simulation. The atoms sputtered from the front surface of the crystal during the simulation are required to have a certain minimum energy. Hence, the sputtering

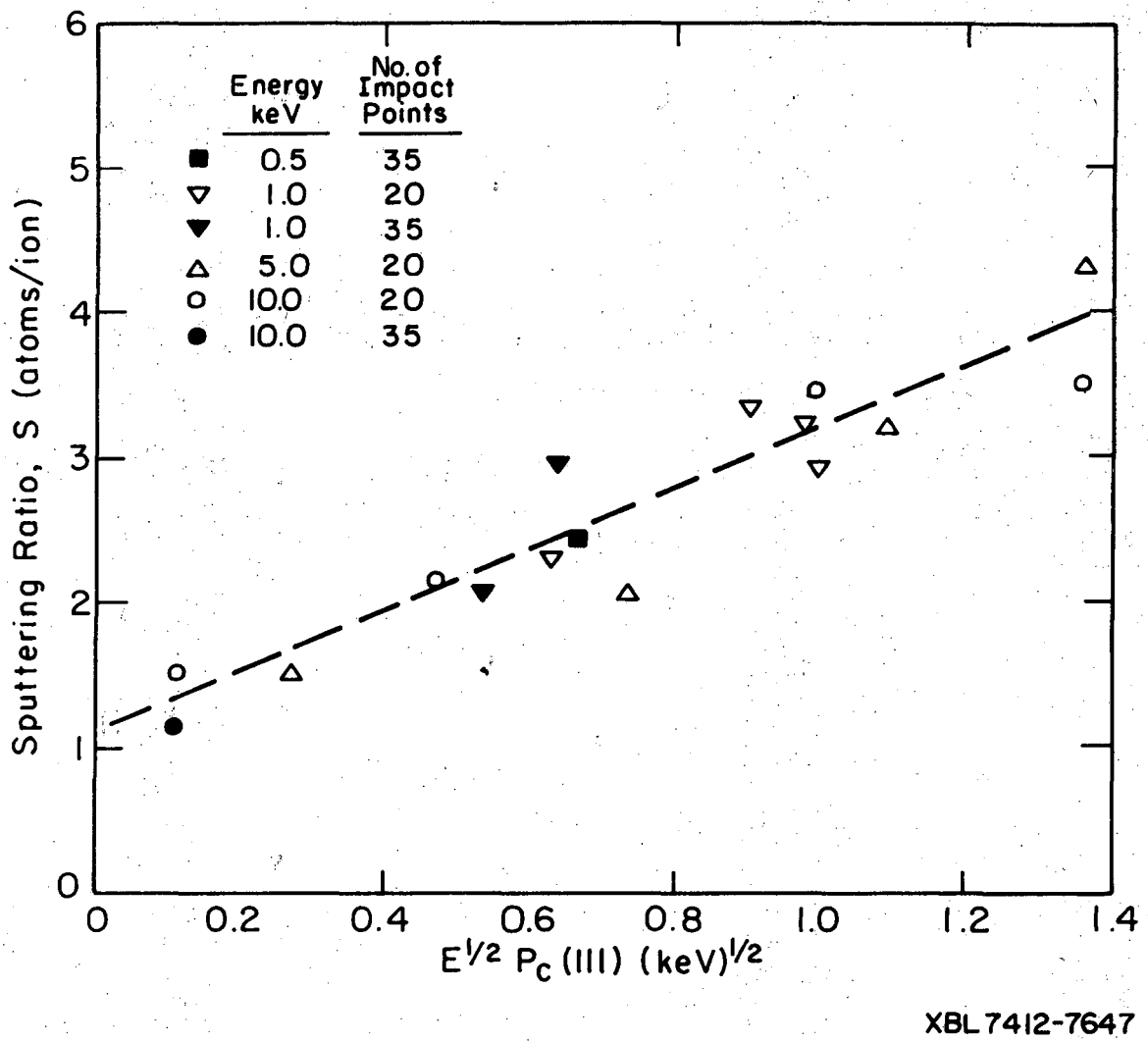

Fig. 8. Simulated sputtering ratio of Ne^+ on (111) copper; plotted against $E^{1/2}$ P_C.

ratio is dependent on the cut-off energy selected. Reduction of this effective binding energy for sputtering would result in a larger number of sputtered atoms, with the increase in the sputter ratio greater for those points where the sputtering ratio is already high. The straight line through all simulation points would now pass closer to the origin with a lower cut-off energy.

(iii) The simulation is not valid for small values of S or P_c. It is not valid because the sputs/ion count is so small that hundreds of impact points would be required to obtain statistical confidence in the S value. It is possible, however, that these values are small in the actual sputtering process.

7. Discussion

The simulation results indicate that

$$S \propto E^{1/2} P_c \tag{7.1}$$

Hence, the mechanism of sputtering that produces such a dependence on ion energy is one of momentum transfer rather than of energy transfer. We can assume that such a law should apply to experimental data.

In Eq. (6.5) the constant K(hkl) can be divided into two terms so that

$$K(hkl) = K'(hkl) P_m \tag{7.2}$$

where P_m accounts for the masses of the incident ion and the target atom. Magnuson et al have pointed out that the variation in sputtering ratio obtained by replacing Cu with Ag as a target material is better explained by using

$$P_m = \frac{2M_2}{(M_1 + M_2)} \tag{7.3a}$$

rather than by using

$$P_m = \frac{4\, M_1 M_2}{(M + M_2)^2} \tag{7.3b}$$

This finding suggests that the sputtering process is controlled by a momentum transfer mechanism, whereas the form of Eq. (7.3b) corresponds to an energy transfer mechanism. It is to be pointed out that since $S \propto E^{1/2}$ we would also expect that $S \propto E_r^{1/2}$, or

$$S \propto \sqrt{\frac{M_2}{(M_1 + M_2)}}\; E^{1/2} \tag{7.4}$$

Also, we would expect that the binding energy of the target material should enter into the constant K(hkl).

Equations in which it is assumed that S in inversely proportional to V_o, the binding energy, have been known to correlate well with experimental data.[16] Assuming such a relationship, then, we propose the following form for the constant K(hkl) in Eq. (6.11):

$$K(hkl) = K''(hkl)\, \frac{1}{V_o} \sqrt{\frac{M_2}{(M_1 + M_2)}} \tag{7.5}$$

where, K"(hkl) depends only on crystal orientation, and V_o is the binding lattice energy of the crystal. By estimating the mean ratio $K(hkl)_{Ag}/K(hkl)_{Cu}$ from Table 7 and comparing this with the value predicted by Eq. (7.5), we obtained $R_K = K(hkl)_{Ag}/K(hkl)_{Cu} = 1.28$. Also, from Eq. 7.5 we obtain $R_K = 1.30$ where it is assumed that $V_{o,Cu} = 75.92$ kcal/mole, and $V_{o,Ag} = 63.42$ kcal/mole.[26] Hence, the agreement of experimental data with Eq. (7.5) is good and, in fact,

is considerably better than that obtained from the expression of Magnuson et al.[10] Hence, it is concluded that, for the limited single crystal sputtering data available, a law of the type

$$S(hkl) = K''(hkl) \frac{1}{V_o} E_r^{1/2} P_c(hkl) \qquad (7.6)$$

holds well at intermediate ion energies.

B. Determination of the Potential Function Parameters from Sputtering Ratio Data for Mono-crystalline Targets.

1. Introduction

In the previous section, a simple expression (Eq. 7.6) was found to apply to the sputtering of single crystal. Since the equation involves the parameters of the potential function, we can expect to use this equation in conjunction with experimental sputtering data to deduce the parameters of the potential function describing interactions between impacting ions and target atoms in the sputtering energy range. In this section such a calculation is performed to determine the potentials describing Cu-Cu interactions.

2. Analysis of the Problem

The object of the calculations presented here is to estimate values for the parameters of the Born-Mayer potential function of the form

$$V(r) = E_o \exp(P_B \cdot r) \qquad (2.1)$$

which describes the repulsive interactions between copper atoms. The parameters E_o and P_B in this expression must be selected so that

(i) The sputtering ratio estimated from the modified Magnuson equation,

$$S(hkl) = K(hkl)\, E_r^{1/2}\, P_c(hkl) \tag{2.2}$$

fits the experimental data.[14] Here, S(hkl) is the sputtering ratio for ions incident on the (hkl) face of copper, and E_r is the reduced ion energy

$$E_r = E[M_2/(M_1+M_2)] \ . \tag{2.3}$$

where E is the incident ion energy, and M_1 and M_2 are the masses of the incident ion and target atom, respectively. For bombardment of mono-crystalline copper by Cu^+ ions, we have the conditions,

$$M_1 = M_2 \qquad\qquad E_r = 0.5E \tag{2.4}$$

The function $P_c(hkl)$ is obtained from Fig. 6, with r equal to the collision radius,

$$r_c = \frac{\ln\,(E_o/E_r)}{(-P_B)} \ . \tag{2.5}$$

The constant factor K(hkl) depends on the mass ratio (M_2/M_1) and also the crystal orientation.

(ii) The contribution of the repulsive forces to the elastic moduli[18] should be in agreement with experiment.[19] Equations (5.1) through (5.4) are used in these calculations and experimental values are listed in Table 5 of Section A.

From the results of Section A we can assume that

$$S \propto E_r^{1/2} P_c \tag{2.6}$$

and

$$P_c \propto (r_c/a)^n \tag{2.7}$$

where $n \approx 1.925$ for a (111) surface. As outlined in Section A.3, we can substitute for r_c in Eq. (2.7) by utilizing Eq. (2.5). This is then substituted into Eq. (6.6) and the resulting expression is differentiated with respect to E_r to obtain an expression for the energy at which the maximum sputtering is expected. Thus,

$$\ln E_r = P_A - 3.850 \quad . \tag{2.8}$$

The experimental S-E curve for sputtering of Cu(111) by Cu^+ ions shows a maximum at about 11 keV. Using this value for $E(-2E_r)$ in Eq. (2.8) we can obtain an estimate of P_A.

Equation (5.1) states that

$$C_{11} = \sqrt{2}\, r_o^{-1} \left[V''(r_o) + r_o^{-1} V'(r_o)\right] \tag{2.9}$$

where $r_o = 2.551$Å, $V(r) = \exp(P_A + P_B \cdot r)$, and $V'(r) = P_B \exp(P_A + P_B \cdot r)$ (eV/1.u.). The potential gradient $V'(r)$ can also be put in the form

$$V'(r) = \frac{P_B}{(1.8075)} \exp(P_A + P_B \cdot r) \ (\text{eV/Å}) \quad . \tag{2.10}$$

Similarly, the second derivative is

$$V''(r) = \left(\frac{P_B'}{1.8075}\right)^2 \exp\,(P_A+P_B\cdot r)\ \text{eV}/(\text{Å})^2 \qquad (2.11)$$

Combining Eqs. (2.10 and (2.11) with Eq. (2.9), with r_o = 2.551Å and simplifying we obtain $C_{11} = 0.1697\ [P_B^{\ 2} + 0.7085\ P_B]\ \exp(P_A+P_B\cdot\sqrt{2})\ \text{eV}/(\text{Å})^3$ or $C_{11}=2.715\times10^{12}\ [P_B^{\ 2} + 0.07085\ P_B]\ \exp(P_A+P_B\cdot\sqrt{2})$ dynes/cm^2. Choosing a value of P_B such that $C_{11}\approx11.0\times10^{11}$ dynes/cm^2 (the experimental value) assures reasonable agreement with experiment (See Table 5). Hence, we obtain the equation

$$(P_B^{\ 2}+0.7085\ P_B)\ \exp(P_A+1.4142\cdot P_B) = 4.0516 \qquad (2.12)$$

Once a value of P_A is chosen by Eq. (2.8), Eq. (2.12) can be solved for P_B by successive approximation.

3. Procedure for Calculations

Two trial potential functions were chosen for initial study. One function, V_{Cu-1}, was set with P_A=12.52 and P_B=-11.24, corresponding to E_r=5000 in Eq. (2.8) or to an experimental maximum sputter ratio at 10 keV. The second function, V_{Cu-2} contained P_A=12.19 and P_B=-10.98, corresponding to E_r=4000 in Eq. (2.8), or to an experimental maximum sputter yield at about 8 keV.

4. Results

The calculated S-E curve are summarized in Table 8 for the potential function V_{Cu-1} and in Table 9 for the function V_{Cu-2}. The predicted sputtering ratios for both potential functions are listed

Table 8. Calculations for V_{Cu-1} (P_A = 12.52, P_B = -11.24)

E(keV)	r_c(l.u.)	(r_c/a)	P_C			$E^{1/2}$ P_C		
			(110)	(100)	(111)	(110)	(100)	(111)
1.0	0.561	0.280	0.69	0.89	1.0	0.69	0.89	1.0
2.0	0.525	0.262	0.60	0.83	1.0	0.74	1.02	1.23
3.0	0.463	0.232	0.48	0.685	1.0	0.83	1.19	1.73
5.0	0.418	0.209	0.39	0.56	0.92	0.87	1.25	2.06
7.5	0.382	0.191	0.32	0.45	0.79	0.875	1.23	2.16
8.0	0.376	0.188	0.31	0.435	0.765	0.880	1.23	2.16
10.0	0.356	0.178	0.275	0.39	0.685	0.870	1.23	2.17
12.5	0.336	0.168	0.245	0.34	0.61	0.866	1.20	2.16
15.0	0.320	0.160	0.225	0.31	0.555	0.871	1.20	2.15
17.5	0.306	0.153	0.205	0.28	0.51	0.858	1.17	2.13
20.0	0.294	0.147	0.19	0.26	0.47	0.850	1.16	2.10
22.5	0.284	0.142	0.18	0.24	0.44	0.85	1.14	2.10

Table 9. Calculations for V_{Cu-2} (P_A = 12.19, P_B = -10.98)

E(keV)	r_c(1.u.)	(r_c/a)	P_C			$E^{1/2}$ P_C		
			(110)	(100)	(111)	(110)	(100)	(111)
1.0	0.544	0.272	0.65	0.87	1.0	0.65	0.87	1.0
2.0	0.481	0.2405	0.51	0.73	1.0	0.72	1.03	1.41
3.0	0.444	0.222	0.44	0.63	0.98	0.762	1.09	1.70
5.0	0.400	0.200	0.352	0.505	0.86	0.787	1.13	1.92
7.5	0.361	0.1805	0.286	0.4	0.73	0.783	1.095	2.0
8.0	0.355	0.1775	0.275	0.388	0.722	0.778	1.097	2.04
10.0	0.334	0.167	0.245	0.335	0.605	0.775	1.059	1.91
12.5	0.314	0.157	0.22	0.03	0.54	0.778	1.061	1.91
15.0	0.298	0.149	0.195	0.265	0.485	0.755	1.026	1.88
17.5	0.284	0.142	0.175	0.24	0.44	0.732	1.004	1.84
20.0	0.271	0.1355	0.16	0.22	0.22	0.405	0.984	1.81
22.5	0.261	0.1305	0.147	0.206	0.38	0.697	0.972	1.80

Table 10. Calculations for V_{Cu-2}, inclusive of the effect of implanted ions.

E(keV)	r_c(l.u.)	(r_c/a)			P_C			$E^{1/2}\ P_C$		
		(110)	(100)	(111)	(110)	(100)	(111)	(110)	(100)	(111)
1	0.544	0.307	0.293	0.282	0.82	0.93	1.0	0.82	0.93	1.0
2	0.481	0.271	0.259	0.249	0.62	0.816	1.0	0.877	1.154	1.414
3	0.444	0.250	0.239	0.230	0.55	0.725	1.0	0.953	1.256	1.732
5	0.400	0.226	0.215	0.207	0.455	0.59	0.907	1.017	1.319	2.028
7.5	0.361	0.204	0.194	0.187	0.37	0.47	0.76	1.013	1.287	2.081
10.0	0.334	0.188	0.180	0.173	0.31	0.40	0.645	0.980	1.265	2.039
12.5	0.314	0.177	0.169	0.163	0.275	0.342	0.575	0.972	1.209	2.033
15.0	0.298	0.168	0.161	0.154	0.246	0.310	0.52	0.952	1.200	2.014
17.5	0.284	0.160	0.153	0.147	0.225	0.280	0.475	0.941	1.171	1.987
20.0	0.271	0.153	0.146	0.140	0.205	0.257	0.43	0.917	1.149	1.923
22.5	0.261	0.147	0.141	0.135	0.190	0.240	0.405	0.901	1.138	1.921

alongside the experimental data[14] in Table 11. Figures 9 and 10 show the results of the simulation for potentials V_{Cu-1} and V_{Cu-2}, respectively. The experimental points are included for comparison.

5. Discussion

From Fig. 9 it can be seen that the curve obtained with the use of the function V_{Cu-1} displays a sputtering ratio maximum at approximately the same energy as for the experimental results on the sputtering of (111) copper by Cu^+ ions. Furthermore, the position of the maxima, for the (111), (100) and (110) faces relative to each other, are in approximately the correct positions.

Figure 10 shows improved agreement with experiment over the situation in Fig. 9. The theoretical curves follow the trend of the experimental points quite nicely for the (110) and (100) faces. For the (111) face, agreement is good for the higher energies. However, the most serious drawback is that the theoretical curve shows a distinct maximum at about 8 keV, while the experimental points seem to indicate a maximum at about 11 keV. One fact is clear, however, and this is that the value of P_A chosen has a strong effect on the position at which the maximum appears in the theoretical curves.

The deviations between the theoretical and experimental curves may be explained on the basis of the following arguments:

(i) The interatomic potential function probably follow a more complex dependence on energy than can be represented by a Born-Mayer potential. The true potential is expected to differ significantly at low energies near the potential energy minimum.

Table 11. Sputtering of monocrystalline copper by Cu^+ ions. Calculated and experimental sputtering ratios (atoms/ion).

E(keV)	Experimental[14]			V_{Cu-1}			V_{Cu-2}			$V^{(a)}_{Cu-2}$		
	(110)	(100)	(111)	(110)	(100)	(111)	(110)	(100)	(111)	(110)	(100)	(111)
1.0	-	-	-	2.61	3.70	4.73	2.88	4.10	5.2	2.85	3.75	4.93
2.0	-	-	-	2.74	4.55	6.69	3.19	4.86	7.33	3.04	4.65	6.96
3.0	-	-	-	3.14	4.93	8.20	3.38	5.14	8.84	3.31	5.06	8.53
5.0	-	-	-	3.3	5.20	9.73	3.49	5.33	10.00	3.53	5.32	10.00
7.5	-	5.5	10.25	3.32	5.12	10.24	3.47	5.17	10.4	3.52	5.19	10.25
8.0	-	-	-	-	-	-	3.46	5.17	10.6	-	-	-
10.0	3.4	5.0	10.50	3.29	5.11	10.25	3.44	5.00	10.0	3.40	5.10	10.04
12.5	3.3	4.95	10.50	3.28	4.99	10.21	3.45	5.00	9.93	3.37	4.87	10.01
15.0	3.4	4.93,4.3	9.95	3.28	4.98	10.17	3.35	4.84	9.78	3.30	4.84	9.92
17.5	3.3	4.5	9.5	3.25	4.86	10.09	3.25	4.74	9.57	3.27	4.72	9.79
20.0	3.25	4.45	9.5	3.22	4.83	9.95	3.18	4.64	9.41	3.18	4.63	9.47
22.5	3.10	4.4	9.325	3.22	4.72	9.88	3.09	4.50	9.36	3.13	4.59	9.46
			K =	3.78	4.15	4.73	4.44	4.61	5.20	3.47	4.03	4.93

(a) taking into account the effect of implanted copper ions.

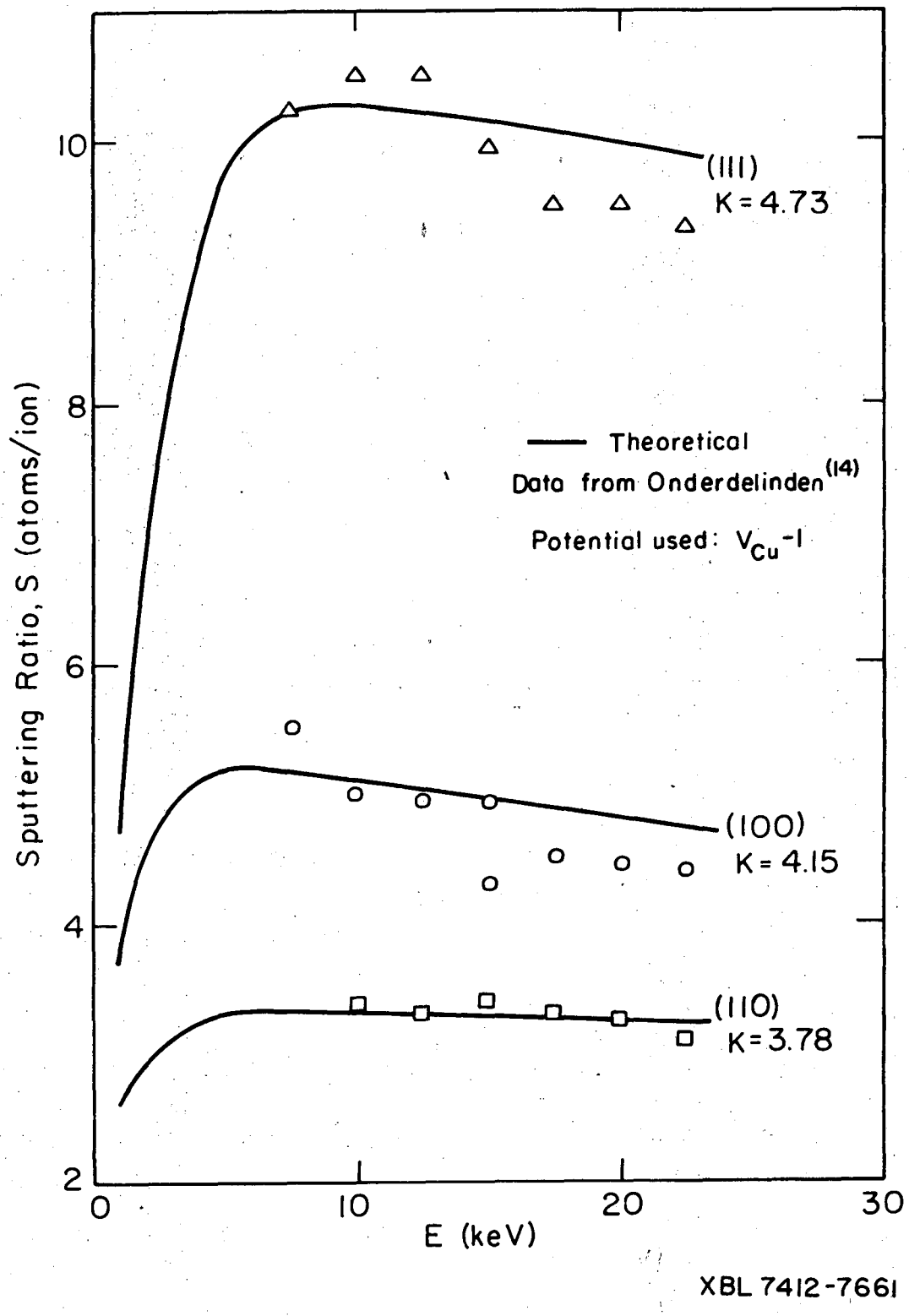

Fig. 9. Graphical comparison of experimental sputtering ratios, for Cu^+ on (111), (100) and (110) copper, with theoretical curves obtained with the use of potential V_{Cu-1} to represent Cu-Cu interactions.

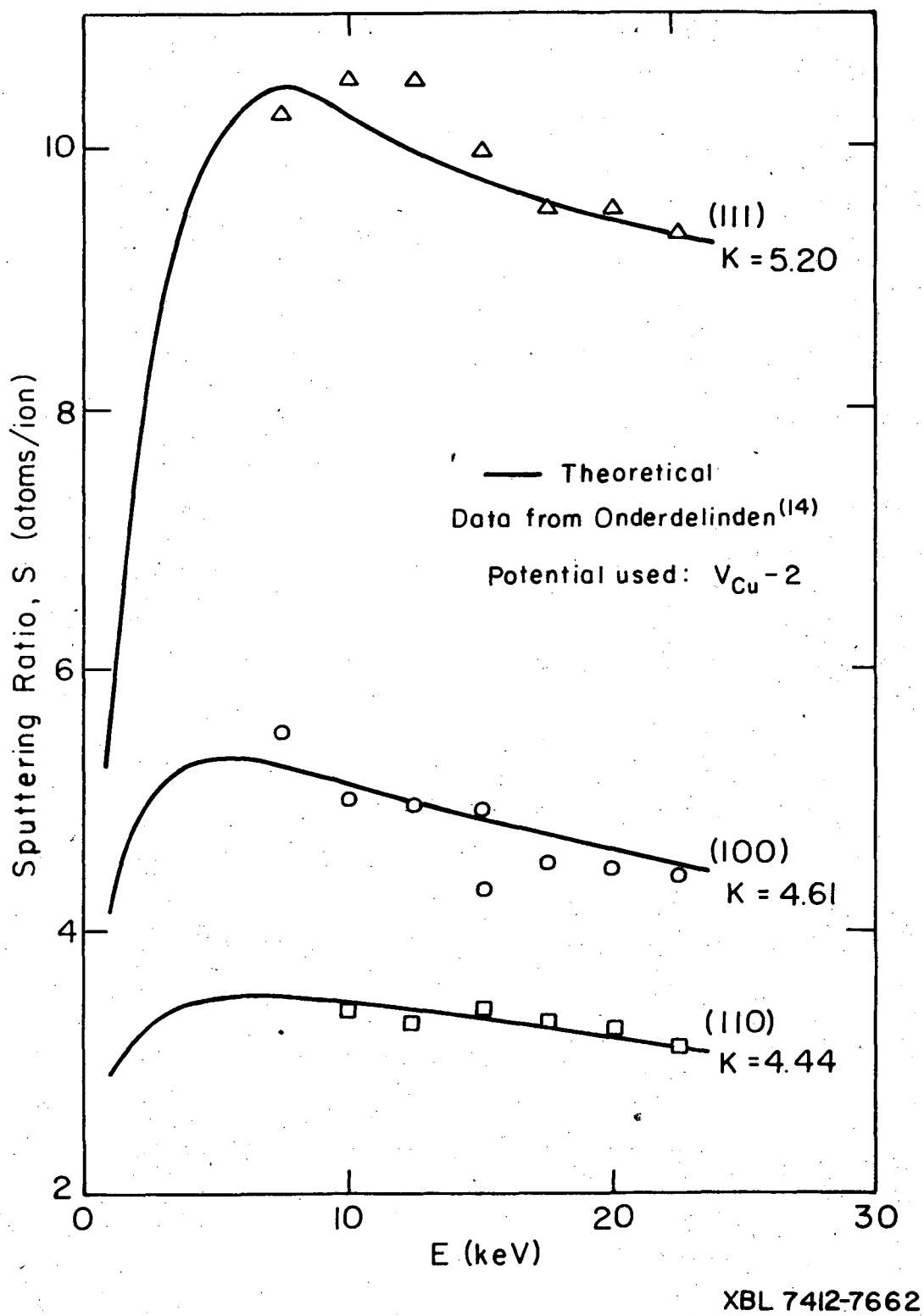

Fig. 10. Graphical comparison of the sputtering ratios, of Cu^+ on (111), (100) and (110) copper with theoretical curves, obtained using potential V_{Cu-2} to represent Cu-Cu interactions.

(ii) The curves for $P_c(hkl)$ have been derived by on the basis of simple geometric considerations. The fact that atoms in different layers have different probabilities of being sputtered has not been taken into account.

In view of the above uncertainties, it is concluded that further calculation with new potential functions was not warranted.

The potentials V_{Cu-1} and V_{Cu-2} give contributions to the elastic moduli which are in reasonable agreement with experimental data. The calculated moduli are indicated in Table 5. The potentials GB-2, V_{Cu-1} and V_{Cu-2} are plotted in Fig. 11. A fourth potential GB-1 is also plotted in this figure for comparison. In their computer simulation study on the dynamics of radiation damage in copper, Gibson et al.[5] found that GB-2 gave displacement threshold energies of approximately the right magnitude, while GB-1 gave displacement thresholds that were too high. Gibson et al. have not given a quantitative estimate of the actual displacement energy for GB-1.

From Fig. 11, V_{Cu-1} and V_{Cu-2} both lie between the GB-1 and GB-2 potentials. It would seem that both should give displacement thresholds which are slightly on the high side. Nevertheless, it should be pointed out that the events of importance in sputtering correspond to relatively high energy interactions between atoms (1-10 keV) while the events studied by Gibson et al. involved atom interactions of lower energy (about 0.4 keV). It is possible the potential functions V_{Cu-1} and V_{Cu-2} are better approximations to the true potential functions for Cu at higher energies (greater than

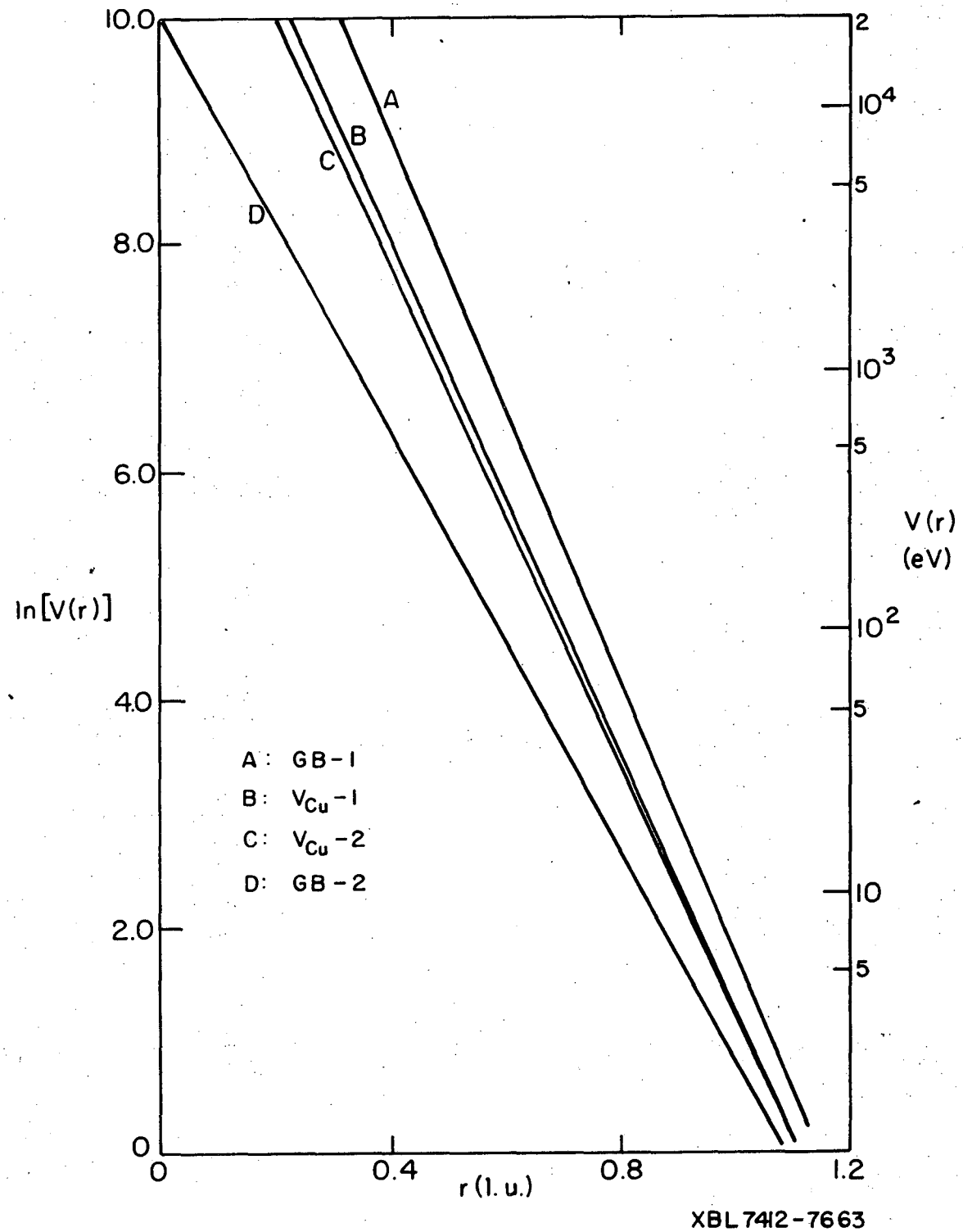

Fig. 11. Graphical comparison of various potentials used to represent Cu-Cu interactions.

5 keV) while GB-2 is a better approximation at lower energies (0.01 to 0.4 keV). This would indicate that the true interatomic potential has a rather more complicated relationship than as represented by a simple Born-Mayer potential. A recent collection of important work on interatomic potentials shows that such a potential curve is certainly feasible.[29] It is also necessary to point out that the shape of the theoretical curves, obtained by the calculations, is not insensitive to the assumed potential function. A relatively small change in the potential function leads to a considerable alteration in the shape of the S-E curves (see Fig. 11 and compare with Figs. 9 and 10).

6. Effect of Entrapped Ions

In the work of Magnuson et al.,[10] where the authors had to introduce a potential function which deviated very significantly from the simple Bohr potentials in order to explain the experimental data, these authors attributed this deviation to the effect of trapped noble gas ions and also to the effect of radiation damage.

In the case of sputtering of copper by Cu^+ ions the effect of gas atom entrapment is not expected since the sputtering ions and target atoms are of the same type. On the other hand, both sputtering processes generate point defect clusters in the target. In any case, it is possible to make some sort of estimate of the effect of these trapped ions or point defect clusters in terms of reduced target density.

In the steady state for sputtering by noble gas atoms, for every incident ion, $(1-x_g)S$ atoms of the original crystal lattice and x_gS trapped gas atoms are sputtered, where S is the sputtering ratio and x_g is the mole fraction of entrapped gas. This means that the effective sputtering ratio decreases with noble gas incorporation if we assume that the trapped gas has the same sputter yield as the lattice atoms. Hence, there is an effective increase in the effective volume per target atom, and an increase in the effective lattice constant. For use in equations predicting sputter ratios in terms of the lattice constant of the target, a, an effective lattice constant can be defined by

$$a_N = a\left(\frac{\text{new volume per target atom}}{\text{original volume per target atom}}\right)^{1/3} = a(1-x)^{-1/3} \quad (6.1)$$

A maximum effect of entrapped gas corresponds to an ion entrapment probability equal to unity. In this case, every incident ion sputters one entrapped gas atom, and $a_N \simeq a[(S-1)/S]^{1/3}$. Using this expression and S=3.3, 5.0 and 10.0 for the (110), (100) and (111) faces of Cu, respectively the simulation calculations for estimating theoretical sputtering ratios were repeated, using the potential V_{Cu-2}. The results are presented in Tables 10 and 11 and in Fig. 12. A comparison of Figs. 12 and 10 shows that the overall shapes of S-E curves, and especially the position of the maxima, are not significantly altered. The proporationality constants K are, however, changed quite noticeably, for the (110) surface which has the lowest sputtering ratio. These calculations show the maximum effect of gas incorporation. Experiments

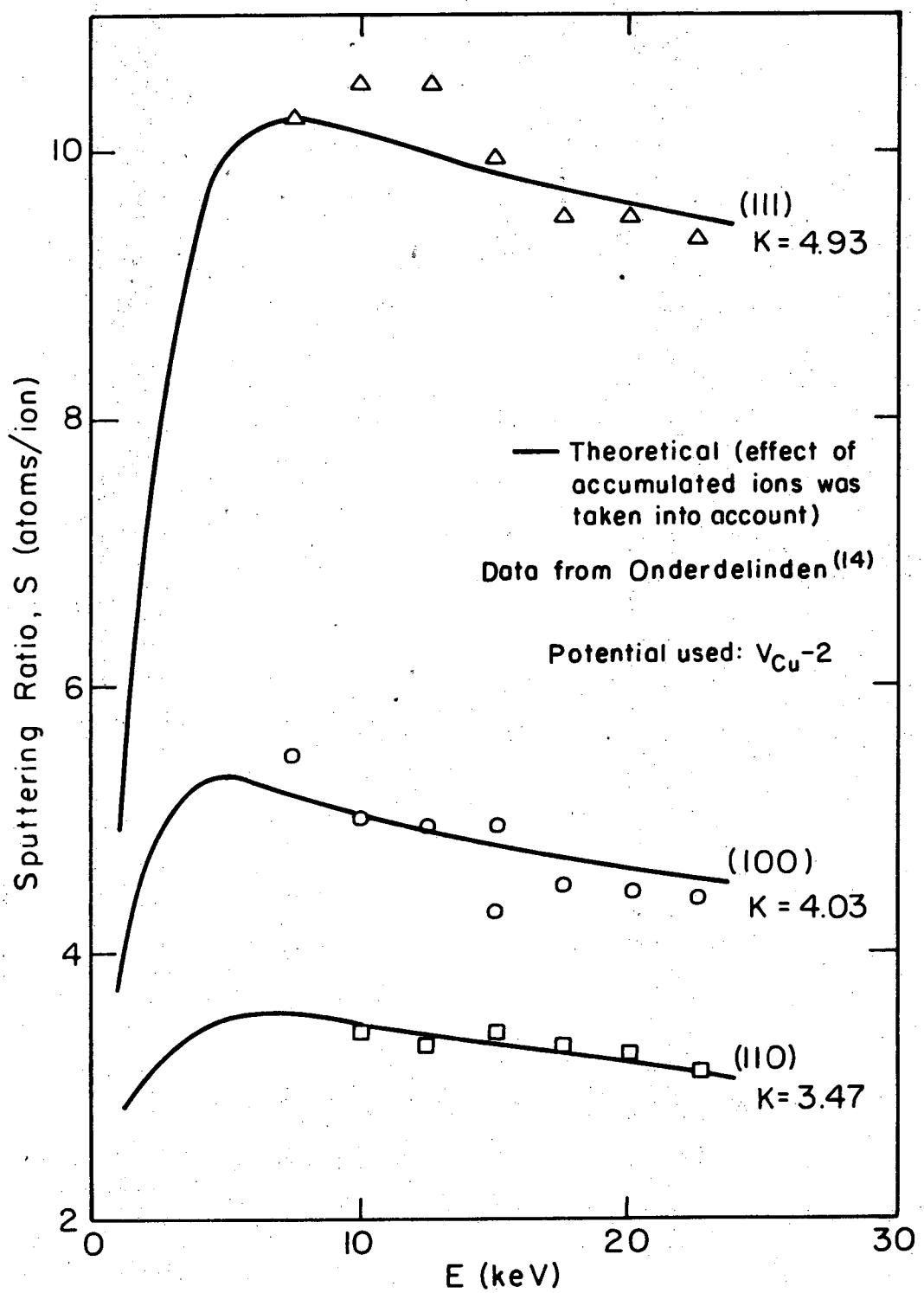

Fig. 12. Graphical comparison of the experimental sputtering ratios for Cu^+ on (111), (100) and (110) copper with values calculated using potential V_{Cu-2} to represent Cu-Cu interactions. The effect of entrapped ions was also taken into account.

have shown that x_g is only on the order of 1-2%. This effect is likely to be even less due to relaxation effects in the lattice. Thus, we may conclude that the effect of the trapped ions is to alter the overall level of the sputtering curves, causing a proportional increase in sputtering ratio at all points. This effect will be stronger for lower sputtering ratios. The overall shape of the S-E curves is, however, not noticeably altered by the trapped ions.

Hence, the potential functions derived from the experimental sputtering data maybe expected to be at least reasonable first approximations to the actual potential function at these energies (5 to 25 keV).

7. Conclusion

It has been demonstrated that it is possible to back-calculate the interatomic potential from the data on the self-sputtering of a single crystal. The calculations show that the position of the maxima in S-E curves correspond to the general trend of the experimental curves. These calculations serve to give important pointers on the nature of interatomic potentials in the energy regions over which sputtering ratio data is available.

The potentials calculated for Cu-Cu interactions in the energy range from 5 to 30 keV do not agree well with the potential functions cited thus far in the literature for Cu-Cu interactions, notably the Gibson potentials. However, the calculated potentials might represent a better approximation to the true potential in the high energy region (5 to 30 keV), while the GB-2 potential could represent a better approximation to the true potential at lower energies (below 400 eV).

REFERENCES

1. D.E. Harrison, Jr., W.L. Moore, Jr. and H.T. Holcombe, Rad. Effects, 17, 167 (1973).
2. D.E. Harrison, Jr., J. Appl. Phys. 40, 3870 (1969).
3. D.E. Harrison, Jr., W.L. Gay and H.M. Effron, J. Math. Phys. 10, 1179 (1969).
4. D.E. Harrison, Jr., J.P. Johnson III, and H.M. Effron, J. Appl. Phys. 39, 3742 (1968).
5. J.B. Gibson, A.N. Goland, M. Milgram and G.H. Vineyard, Phys. Rev. 120, (4), 1229 (1960).
6. H.B. Huntington and F. Seitz, Phys. Rev. 61, 315 (1942).
7. H.B. Huntington, Phys. Rev. 91, 1092 (1953).
8. G. Carter and J.S. Colligon, "Ion Bombardment of Solids", American Elsevier Publishing Co., pp. 314 (1968).
9. A.L. Southern, W.R. Willis and M.T. Robinson, J. Appl. Phys. 14 (1), 153 (1963); M.T. Robinson and A.L. Southern, J. Appl. Phys. 38, (7), 2969 (1967).
10. G.D. Magnuson and C.E. Carlston, J. Appl. Phys. 34, (11), 3267 (1963).
11. J.J. Ph. Elich, H.E. Roosendaal, D. Onderdelinden, Rad. Effects, 14, 93 (1972).
12. J.J. Ph. Elich, H.E. Roosendaal, H.H. Kersten, D. Onderdelinden, J. Kistemaker and J.D. Elen, Rad. Effects 8, 11 (1971).
13. D. McKeown and A.Y. Cabezas, Annual Report Space Sci. Lab., General Dynamics/Astronautics, (1962).
14. D. Onderdelinden, Can. J. Phys. 46, 739 (1968).

15. O. Almen and G. Bruce, Nucl. Instr. Methods, 11, 257 (1961)

16. P. Sigmund, Phys. Rev. 184 (2), 383 (1969).

17. A.A. Abrahamson, Phys. Rev. 178, 76 (1969).

18. H.B. Huntington, in Solid State Physics, edited by F. Seitz and D. Turnbull (Academic Press Inc., New York, 1958), 7, p. 213.

19. W.C. Overton, Jr. and J. Yaftney, Phys. Rev. 98, 969 (1955).

20. H. Anderson and P. Sigmund, Nucl. Instr. Methods 38, 238 (1965). Danish Atomic Energy Commission Risø Report No. 103, 1965 (Unpublished).

21. N. Bohr, Mat. Fys. Medd. Dan. Vid. Selsk 18, 8 (1948).

22. "American Inst. of Phys. Handbook," Second Ed. (1963), D.E. Gray, Coord. Ed. pp 3-7.

23. M.T. Robinson and O.S. Oen, Phys. Rev. 132, (6), 2385 (1963).

24. O.B. Firsov, J. Exp. Th. Phys. 33, 696 (1957) (Transl. 6, 534 (1958)).

25. J. Lindhard, V. Nielsen, and M. Scharft, Mat. Fys. Medd. Dan Vid. Selsk. 36, 10 (1968).

26. P. Gombas in 'Encyclopedia of Physics' Springer (1956), p. 109.

27. Perry's Handbook, pp. 498 and 501.

28. E.B. Henschke and S.E. Derby, J. Appl. Phys. 34 (8), 2458 (1963).

29. 'Interatomic Potentials and Simulation of Lattice Defects', edited by P.C. Gehlen, J.R. Buler, Jr. and R.I. Jaffee, Plenum Press, New York (1972).

30. G. Dupp and A. Scharmann, Z. Physik, 192, 284 (1966).

SYMBOLS

AB-Ar-Cu: Abrahamsons[17] recommended potential function for Argon-Copper interactions. (Text: , Table 4)

AB-Cu: Abrahamsons[17] recommended potential function for copper-copper interactions.

AB-Ne-Cu: Abrahamsons[17] recommended potential functions for Neon-Copper interactions. (Text: , Table 4)

A_o: Parameter in the potential function recommended by Anderson et al.[20]

a: Unit all length. (=3.615Å for Cu)

a_A: Parameter in the potential function recommended by Anderson et al.[20]

a_B: Parameter to be used with Bohr's interatomic potential (Å). (Text: Eq. A.6-5)

a_F: Firsovs[24] modification to parameter a_B, to be used instead of a_B with the Bohr interatomic potential (Å).

a_L Lindhards[25] modification to be used instead of a_B in the Bohr interatomic potential (Å). (Text: Eq. A.6-5).

a_N: Effective lattice constant, taking into account the effect of trapped ions (Å).

a_o: Bohr radius of the hydrogen atom (=0.529Å).

B: Bulk modulus for metallic copper (dynes/cm^2).

C: Adjustable parameter used in the theory of Magnuson et al[10]

$\left.\begin{matrix} C_{11} \\ C_{12} \\ C_{44} \end{matrix}\right\}$ Elastic moduli for metallic copper (dynes/cm^2)

C(hkl): Proportionally constant in the equation expressing P_c(hkl) as a function of (r_c/a). (hkl) refers to the pertinent monocrystal face. (Text: Eq. A.7-6)

E: Energy of the impacting ion (keV).

E_d: Displacement Energy. Minimum energy needed to displace a lattice atom from its position at a lattice point.

E_o: Pre-exponential factor (keV).

E_r: Energy of the impacting ion in center of mass coordinates (keV). (Text: Eq. A.5-2)

e: Charge of an electron (-1.6×10^{-19} coulomb)

GB-1: Gibson-1 potential function[5] for Cu-Cu interactions. (Text: Fig. A.8-3)

GB-2: Gibson-2 potential function[5] for copper-copper interactions.

h: Plancks constant ($=6.624\times10^{-27}$ erg-sec)

K_1: Constant used in the equation that expresses the sputtering ratio as a function of incident ion energy and hard-sphere radius. (As obtained from the computer simulation) (Text: Eq. A.7-11)

K(hkl): Proportionally constant in equation expressing sputtering ratio S, as a function of ion energy, E, and the probability for ion-atom collisions in the surface layers, P_C. (Text: Eq. (A.7-5))

K"(hkl): Proportionality constant, in the equation used for expressing sputtering ratio S(hkl) as a function of V_o, E_r, and P_c.

k: Adjustable parameter used in the theory of Magnuson et al.[10]

l.u.: Lattice unit. Unit of length. One lattice unit is one half the unit cell legnth 'a' (1 l.u. = 1.8075Å for Cu).

M_1: Mass of the incident ion.

M_2: Mass of the target atom.

m: Mass of electron ($=9.108\times10^{-8}$ gms)

n: Index of 'r_c' indicating variation of sputtering ratios with the hard-sphere radius r_c.

n_x: Denotes value of index n for a monocrystalline target when x=m and for a polycrystalline target when x=p.

n(hkl): Exponents in the equation expressing P_C(hkl) as a function of (r_c/a). (Text: Eq. A.7-6)

P_A: Parameter of potential function V.

P_B: Parameter of potential function V.

V_n: n is an integer which may take on a value from 1 to 9 inclusive. V_n is a name given to one of the potential functions used in the simulation.

P_C(hkl): Probability of an ion making an impact in the first two layers of the crystal. The ion is normally incident on the (hkl) face of the monocrystal (Text: Fig. A.7-4)

p_m: Factor takes into account the effect of variation of the mass of the ion or target atom. (Text: Eq. A.7-14)

$R_{H\cdot C}$: Hard sphere radius for atom-atom interactions as calculated by Magnuson et al.[10] (Text: pg. , Eq. A.7-10)

r: The distance between two interacting atoms. (l.u.).

r_c: Hard sphere radius of atoms (l.u.) (Text: Eq. A.5-3)

r_o: Nearest neighbor distance.

S: Sputtering ratio (atoms/ions)

S-E curve: Curve showing the variation of the sputtering ratio with the energy of the incident ion.

S_o: Constant used in the equation expressing the sputtering ratio (as obtained by use of the simulation) as a function of the incident ion energy E and hard sphere radius r_c. (Text: Eq. A.7-11)

S_x: x is the symbol for an element x. S_x denotes the sputtering ratio when x is the bombarding ion (Ex: S_{Ne}, S_{Ar}, etc.) (Atoms/ion)

$S_{(hkl)}$: Sputtering ratio of the (hkl) face of the mono-crystal (atom/ion).

t: time (sec.)

Δt: Small time increment (sec.)

t_m: Factor to take into account the effect of variation of the mass of the ion on the target atom. (Text: Eq. A.7-15)

V_o: Binding energy of an atom (kcal/g-mole of atoms)

V(r): Potential function. Gives the potential energy of interaction of two atoms with each other (e.V.). r is the distance between the atoms in lattice units (l.u.).

V'(r): First derivative of V(r) with respect to $r\cdot[(e.V.)/(l.u.)]$

V"(r): Second derivative of V(r) with respect to $r\cdot[(e.V.)/(l.u.)^2]$

Z_1: Atomic no. of incident ion.

Z_2: Atomic no. of target atom.

Δt: Small increment in time t sec.

ε_o: Permittivity of free space ($=1/(36\pi\times10^9)$ rationalized M.K.S. units)

PART II: COMPUTER SIMULATION OF OBLIQUE INCIDENCE SPUTTING OF (100) Cu BY Ne^+

ABSTRACT

A computer simulation model was used to simulate the sputtering of (100) Cu by 10 keV Ne^+ ions at incident angles of 20° to 50° from the surface normal. This work extends the earlier investigations by Harrison et al. who studied oblique incidence sputtering of (100) Cu by Ar^+.

The simulation predicts a variation of the sputtering ratio with the angle of ion incidence which shows maxima and minima in the same relative positions to each other as observed experimentally. However, the simulated maxima and minima are shifted about 5° toward the surface normal as compared to the experimental values. This shift is due to use of only one quarter the true representative area for oblique incidence sputtering. A similar shift was found in Harrison's[2-7] work on the simulation of Ar^+/Cu sputtering.

The submaximum at 39° is also obtained by the simulation in the appropriate position relative to the simulated maxima and minima. This peak is stronger for Ne^+/Cu sputtering simulations than for Ar^+/Cu sputtering simulations.

I. INTRODUCTION

A computer simulation model offers greater controllability and observability as compared to experiment. This is because the imputs to the model span a continuum of values as opposed to discrete experimental values, and can be easily varied. If the model is capable of explaining all known experimental results then it can be said that a fundamental understanding of the modelled system has been obtained. It may then be possible to use this model to predict what could happen under circumstances for which experimental data is not yet available. Herein lies the key utility value of computer simulation.

The sputtering of a monocrystalline target by an impacting ion is amenable to such a treatment, within certain limitations imposed by the computer, such as execution time and computer storage.

It is also possible to follow the trajectories of individual atoms and hence obtain a picture of the actual sputtering process, thus leading to the possibility of identifying specific mechanisms which are of interest in sputtering. Such as investigation by Harrison et al.[2-7] has shown that focusons are unimportant in the sputtering process, even for single crystal targets. As shown in Part I of this thesis, it is possible to vary the parameters governing atom-atom interactions and note the effect of these variations on the sputtering ratio. Following such a systematic pattern of study, then, it should be possible to eventually link the variation of the sputtering ratio to all the various factors that can be expected to influence it.

Harrison et al. have done much work on the computer simulation of normal and oblique incidence sputtering of monocrystalline copper by Argon. These studies point to the need for investigations of sputtering by lighter ions where properties of the interatomic potential function are expected to be significant. In this study the simulation model was extended to Ne^+/Cu sputtering. The useful information that was to be gained is outlined as follows:

(i) The effect of the smaller mass of the Ne^+ ion was tested to determine whether there is any significant change in the sputtering mechanism.

(ii) The primary variations in sputtering ratio with incident angle of the impacting ion was predicted by computer simulation to determine whether the simulation is capable of reproducing experimental data.[1]

(iii) Simulation models were tested to determine whether the simulation was capable of reproducing the secondary variations in sputtering ratio with incident angle. These secondary variations are uniquely displayed by the Ne^+/Cu system.[1]

(iv) Simulation results were examined, to identify the mechanism causing the existence of the phenomenon of secondary sputtering ratio variation with incident ion angle.

Experimental data on the oblique incidence sputtering of (100) Cu by Ne^+ is available from the thorough investigations of Elich et al.[1] Their results are presented in detail in Section 2 below. It is sufficient to simply note here that these authors determined the

variation of the sputtering ratio with the angle of incidence of the incidence ion and demonstrated conclusively that some secondary effect gives rise to a secondary submaximum in the S-E curve at angles of the incident ion beam near 39° to the target surface normal. The failure is unique to the Ne^+/Cu system. The nature of the mechanism causing the existance of this submaximum is not clearly understood.

As outlined in the first few paragraphs of this introduction it was hoped that the unique controllability and observability of computer simulation could be used to answer the above unanswered questions.

2. Summary of Relevant Experimental Results from the Literature

Several authors have studied the sputtering of monocrystals by ions and have found that the sputtering ratio varies with the angle of incidence of the incident ion in the following ways:

(i) Firstly, the greater the angle (with respect to the surface normal) at which the ion enters the crystal, the closer the ion-target atoms collisions are to the surface. For such collisions the probability of sputtering is increased.

From much experimental work on polycrystalline materials, the variation of the sputtering ratio, S, with the incident angle ϕ, measured from the surface normal, has been found to follow the law:[12]

$$S(\phi) = S(0)\ [\cos\phi]^{\alpha} \qquad (2.1)$$

where $\alpha \approx -1$. At high angles of incidence (80°), the probability of reflection of the incident ions from the crystal surface becomes appreciable and the observed $S(\phi)$ variation deviates appreciably from Eq. (2.1) above.

(ii) In single crystals, in addition to the inverse cosine dependence of the sputtering ratio, the sputtering ratio also depends on the orientation of the crystal surface exposed to the incident beam. If the crystal is imagined to be made up of atoms of constant radius it will appear to be more transparent when viewed in some directions (low-index directions) and more opaque when viewed in other directions. The experimentally obtained sputtering ratio dependence on the angle of incidence of the incident ion, $S(\phi)$ curves display maxima at angles corresponding approximately to the opaque directions and minima at angles approximately corresponding to the low index directions as shown in Fig. 1.

The above two considerations form the basis of the Transparency theory[9] which can explain the general trends and shapes of the experimentally obtained curves. However, experimental data have been collected which show that various submaxima are also obtained in these curves[1,10] which cannot be explained on the basis of the transparency theory alone.

Onderdleinden studied the dependence of the sputtering ratio of monocrystal targets, on the incident ion energy. As an extension of Onderdelinden's work[8] Elich et al., studied the sputtering of (100) Cu by 20 KeV and 10 keV Ne^+ and 20 keV Ar^+ ions. The (100) surface copper single crystal was rotated about an ⟨001⟩ axis on the surface and the

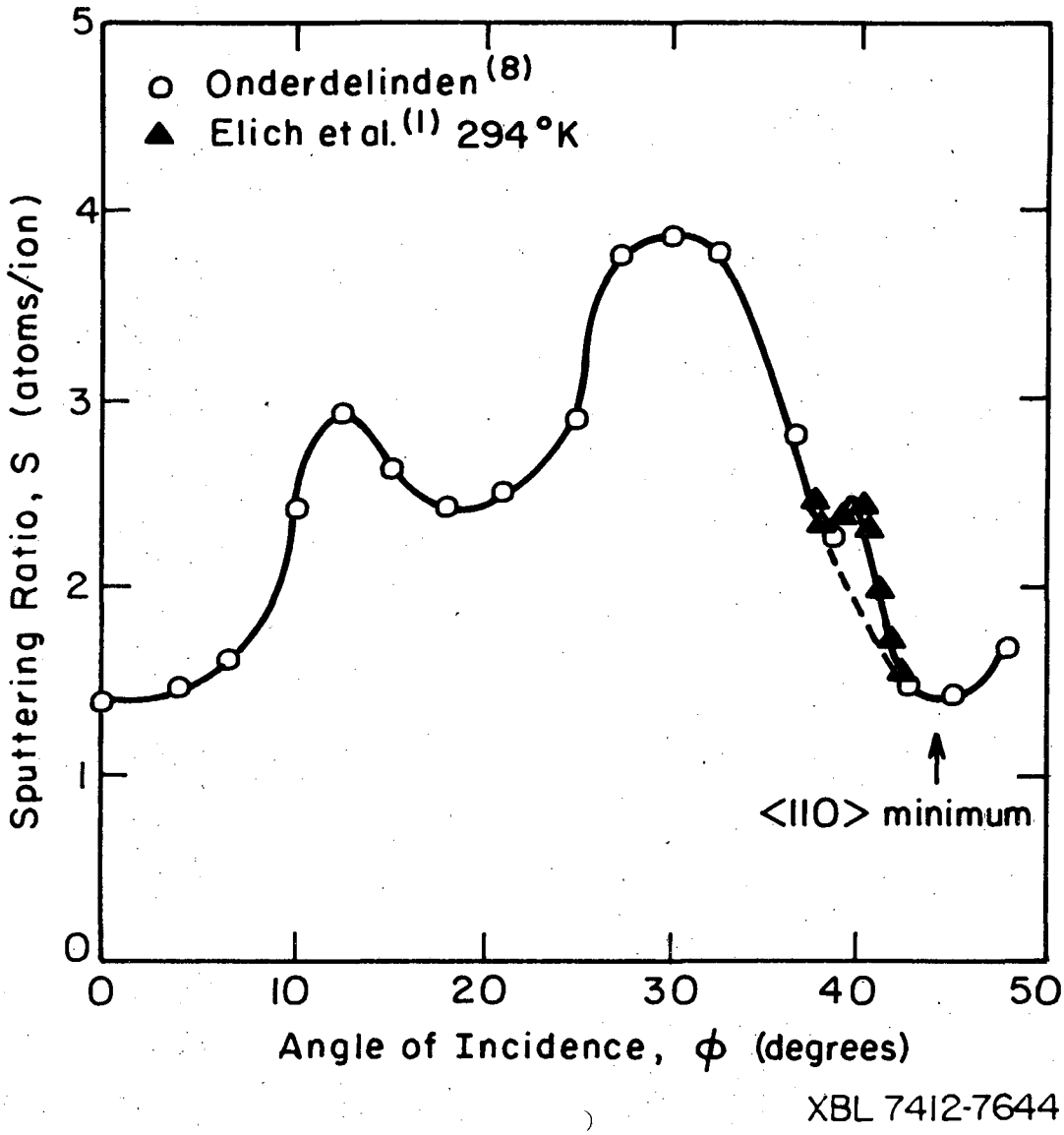

Fig. 1. Sputtering ratio of 20 keV Ne^+ bombarding a (100) Cu crystal turned around a ⟨001⟩ axis in the surface.

variation of the sputtering ratio with the incident angle was measured. The data were obtained at three different temperatures (204°K, 294°K, 456°K). The data showing the variation of the sputtering ratio with the angle of incidence of the incident ion is shown in Fig. 1. This curve clearly displays the major maxima at 12.5° and 30° and the major minima at 0°, 18° and 43°. A small submaximum is also displayed at 39°. This submaximum is of the type mentioned above. Details of this submaximum are displayed in Fig. 2. By studying these figures carefully the following conclusions were arrived at.

(i) As the temperature increases, the submaximum moves towards the ⟨110⟩ minimum and also decreases in magnitude until it disappears at a temperature above 500°K.

(ii) As the ion energy increases, the magnitude of the submaximum increases and moves further away from the ⟨110⟩ minimum. Further, the submaximum is more persistent and remains evident till higher temperatures.

(iii) No clear submaximum is obtained when Argon is used instead of Neon.[1] Thus, the lighter atomic mass of the Ne^+ ion is needed for obtaining this effect.

(iv) It has been found that when sputtering of the monocrystal was carried out at angles of incidence within the interval over which the submaximum extends, a very characteristic systematic surface structure is developed on the surface of the monocrystal. The surface becomes covered with parallel furrows which extend on the surface in the ⟨001⟩ direction perpendicular to the direction of the incident

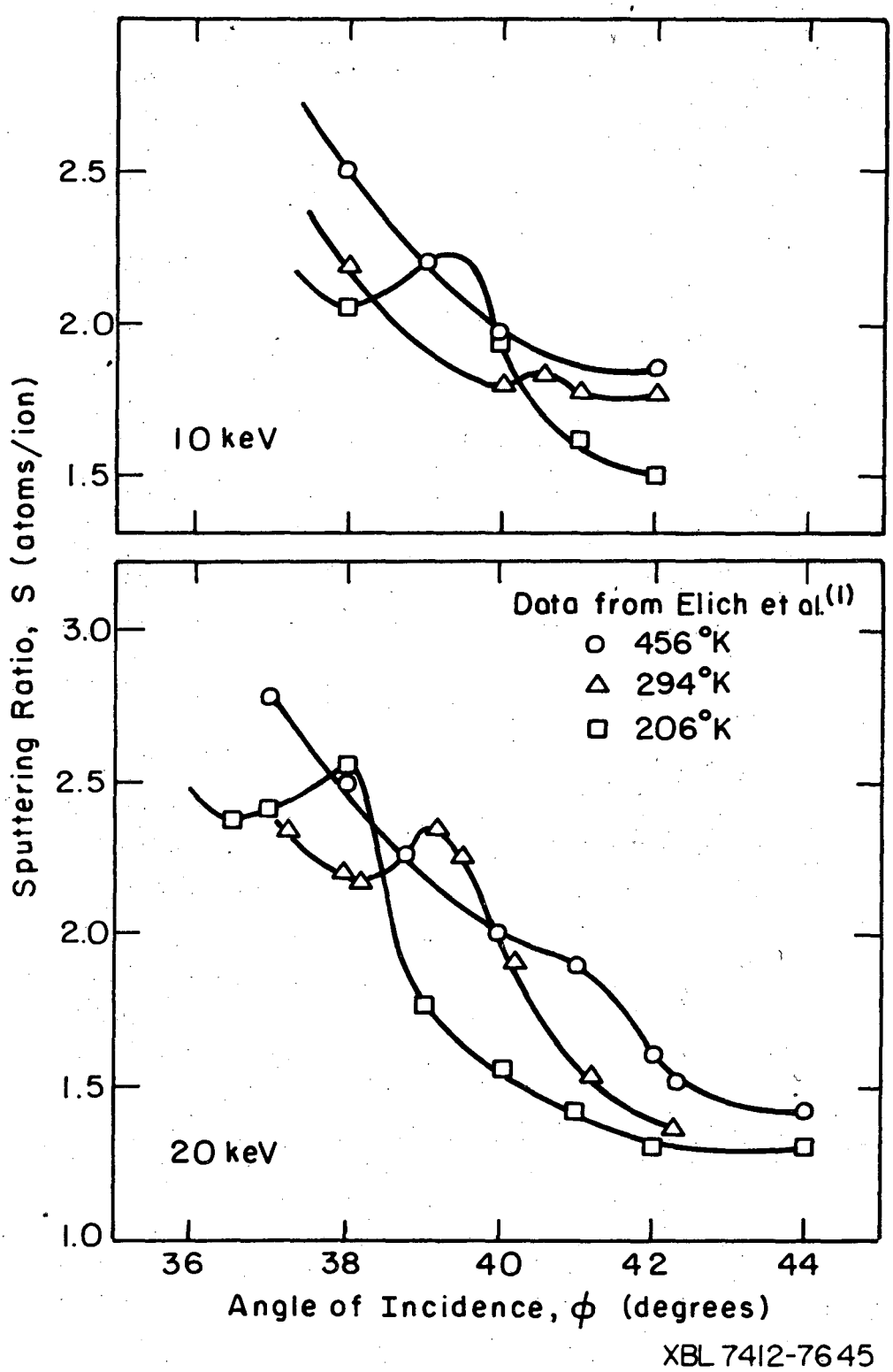

Fig. 2. Sputtering ratio for Ne^+ ions on a (100) Cu crystal turned around a ⟨001⟩ axis in the surface.

beam (and parallel to the axis on the surface about which the crystal was rotated). These parallel furrows were about 0.5μ to 1μ apart and about 0.3μ deep. The furrows become deeper and closer together at angles corresponding to the tip of the submaximum [Fig. 1].

A cross-section of a representative furrow is shown in Fig. (3-a). The direction of the incident ion beam is indicated by arrows. As is indicated in the figure, one of the sides of the furrow corresponds to the (110) surface. The ion beam is at near grazing incidence to this surface.

3. Theory

Elich et al.[1] proposed a simple theory to explain their experimental results. An incident ion was assumed to channel through the target lattice as indicated in Fig. (3-b). As the ion close to a particular string of atoms, along the ⟨110⟩ direction, as shown in the figure, the major interactions are assumed to occur between the ion and this string of atoms. Elich et al.[1] formulate a set of differential equations to describe the trajectory of the ion alongside the atom string. A mathematical expression for the potential between the atom string and the ion assumed and the differential equations were solved, to obtain the trajectory of the ion. The momentum transferred by the ion to an atom in the string, and the direction of that momentum, estimated. If the angle which this momentum makes with the ⟨110⟩ axis small enough, and the transferred momentum large enough, a collision chain in the ⟨110⟩ direction be generated. The probability of such an event estimated by

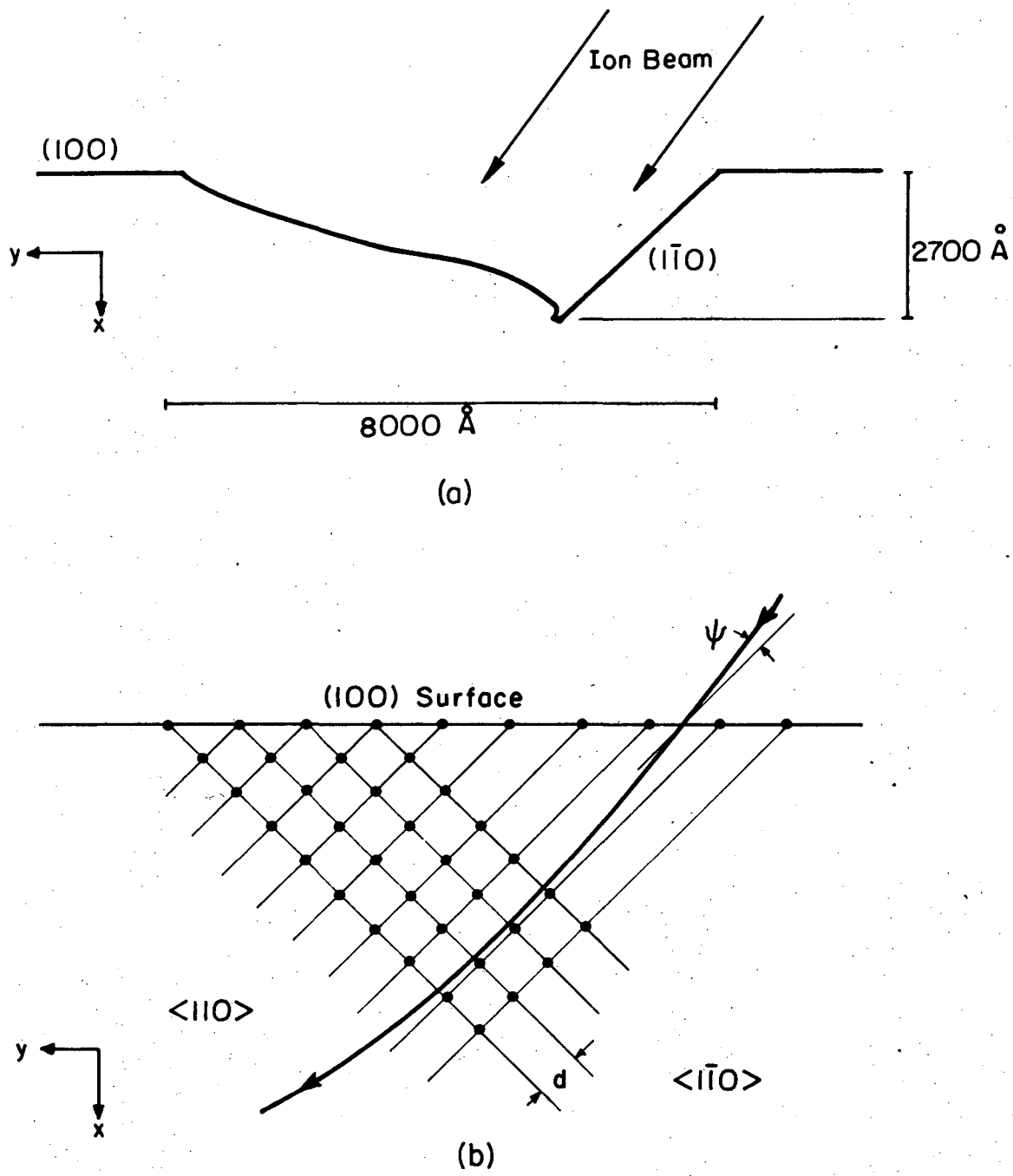

XBL 7412-7646

Fig. 3. (a) Schematic profile of a 'pit' or furrow.
(b) The trajectory of a particle in the (001) plane.

calculating a focusing parameter, λ. A focuson be generated if λ less than 1. Using the expression for λ given by Lehman and Liebfried[11] and taking the focusing energy $E_f^{(110)}$ to be 36 eV and the replacement energy $E_r^{(110)}$ to be 9 eV, Elich et al.[1] obtain an expression for ΔZ, the interval over the atom string in which the incident ion generates focusons perpendicular to the atom string. The angle between the incident ion beam and the ⟨110⟩ direction, ψ, [See Fig. (3-b)] enter into this expression. The angle ψ, corresponding to a maximum value of $(\Delta Z/d)$, corresponds to those angles at which there is high probability for focusons to be generated and directed into the crystal in the ⟨110⟩ direction. These focusons cause dislocations on the surface to appear due to the inward displacement of atoms.

Elich et al.[1] propose that preferential sputtering occurs at these dislocations. The shallow furrows thus formed are eroded deeper as sputtering proceeds. Calculations show how this inward erosion of the furrows is expected to occur. The steady state cross-section of the furrow is shown to have a (110) face for the face that is at near-grazing incidence to the incident beam. The sputtering ratio on a surface at grazing incidence of the incidence ion is much larger than the sputtering ratio at normal incidence. Hence, the formation of the facets causes an increase in the sputtering ratio.

Elich et al. plot the variation of $(\Delta Z/d)$ with ψ at various ion energies and note the magnitude and direction of the shift in the position of the maxima, as ion energy is increased. Unfortunately, the theory predicts a shift towards the 43° minimum as ion energy is

increased, a prediction that is exactly opposite to the observed experimental behavior.

4. Simulation Method and Procedure

Oblique incidence sputtering of mono-crystalline copper by 10 keV Neon has been simulated using the simulation model of Harrison et al.[2-7] This simulation model is described in the Appendix.

The simulation model was used to determine the sputtering ratio at various angles of incidence from 20° to 50°. These simulated sputtering ratios were then compared with experimental values at these angles.

In the simulation runs that were carried out, only the representative area for normal incidence sputtering was used. This is only one-quarter of the representative area that should be used for oblique incidence sputtering as shown in Fig. 2.b of the Appendix. However, it was hoped that such a representative area would still be useful, since it had been found successful in the simulation of oblique incidence sputtering with Argon,[1] and would most significantly decrease the computing time required.

5. The Potential Function

The simulation requires the specification of the potential functions describing the Cu-Cu and Ne^+-Cu interactions. The energy of interaction between two atoms a distance 'r' from each other is given by the Born-Mayer potential function,

$$V(r) = \exp (P_A + P_B \cdot r) \tag{5.1}$$

where P_A, P_B are parameters of the potential function.

In Part I of this thesis it was found that when potential V9 was used with the computer simulation, the predicted variation of sputtering ratio with incident ion energy for normal incidence sputtering of (111) Cu by Ne^+, gave reasonable agreement with experiment. A comparison of the above-mentioned prediction with the use of different potentials is given in Fig. 2 of Part I of this thesis. It is clear that potential V9 gives the best agreement with experimental results. Hence, V9 was selected for the simulation study of oblique incidence sputtering of (100) Cu by Ne^+ to represent interactions between Ne and Cu atoms. The GB-2 potential function was used to represent interactions between Cu atoms. The parameters P_A and P_B for V9 (P_A = 12.5, P_B = -12.71) and GB-2(P_A = 10.0241, P_B = -9.1967) are listed in Tables 6 and 4, respectively, of Part I.

6. Simulation Results and Discussion

The simulated sputtering ratios for 10 keV sputtering of (100) Cu by Ne^+, and the experimental data at 10 and 20 keV, are plotted in Fig. 4. The data at 20 keV gives a qualitative picture of the variation of the sputtering ratio and it can be seen that the simulation results give a minimum and a maximum that are shifted toward smaller angles by about five degrees. This agrees with similar results obtained by Harrison et al.[2] for Ar^+/Cu sputtering simulation who also used

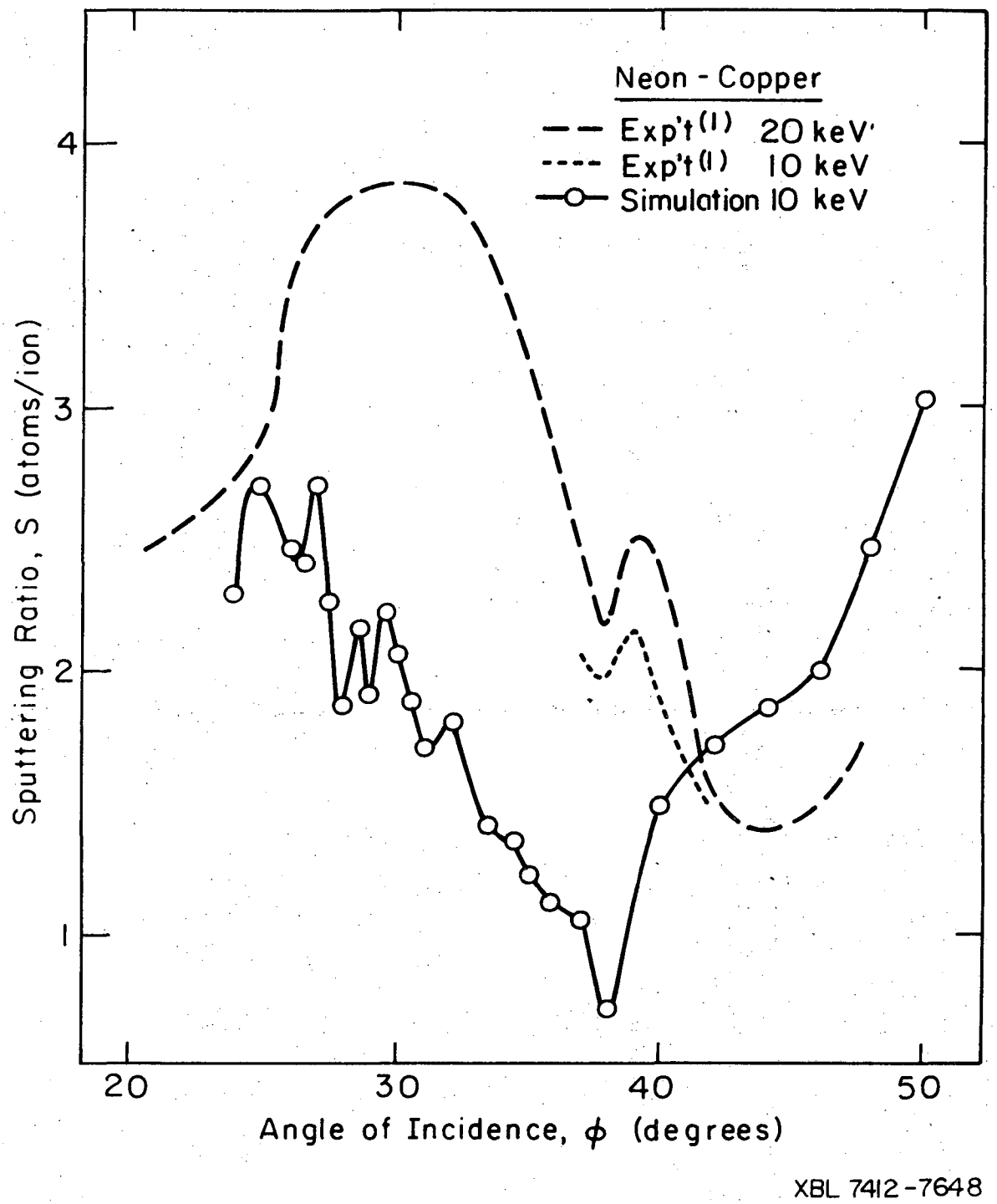

Fig. 4. Experimental and simulation sputtering ratios of Ne^+ on (100) Cu rotated about a ⟨001⟩ axis in the surface.

the same representative area on the crystal surface. Their results are presented in Fig. 5. The reason for the displacement of both results can be traced to the use of only one-quarter of the true representative area for oblique incidence sputtering. Using only one-quarter of the true representative area changes the effective opacity of the crystal to the incident ions. Note the similarities between the simulation results in Fig. 4 and 5.

If the simulation data points obtained in this study are shifted up by about 5° to larger angles to correct for the effect of using a smaller representative area, the simulation and experimental curves agree more satisfactorily. The magnitude of the simulated sputtering ratio submaximum at 39° is comparable to the experimental submaximum.

The scatter in the simulation points for Ne^+/Cu sputtering is large. This makes conclusions regarding the simulation of the 39° submaximum difficult. However a comparison of Figs. 4 and 5 show that a submaximum is indeed obtained in both simulation curves at the approximate location between the simulated maximum at about 25° (corresponding to the experimental maximum at 30°) and the simulated minimum at about 39 to 40° (corresponding to the experimental minimum at about 43 to 44°). These two simulated peaks are magnified in Figs. 6 and 7 for comparison. The similarity in the two peaks is evident, with a tendency for the simulated peak for Ne^+/Cu to be larger than the peak for Ar^+/Cu (relative to the overall sputtering ratio at this point). Considering the crudeness of the model and the several approximations that have been made, the agreement between the experimental results and the simulation is satisfactory.

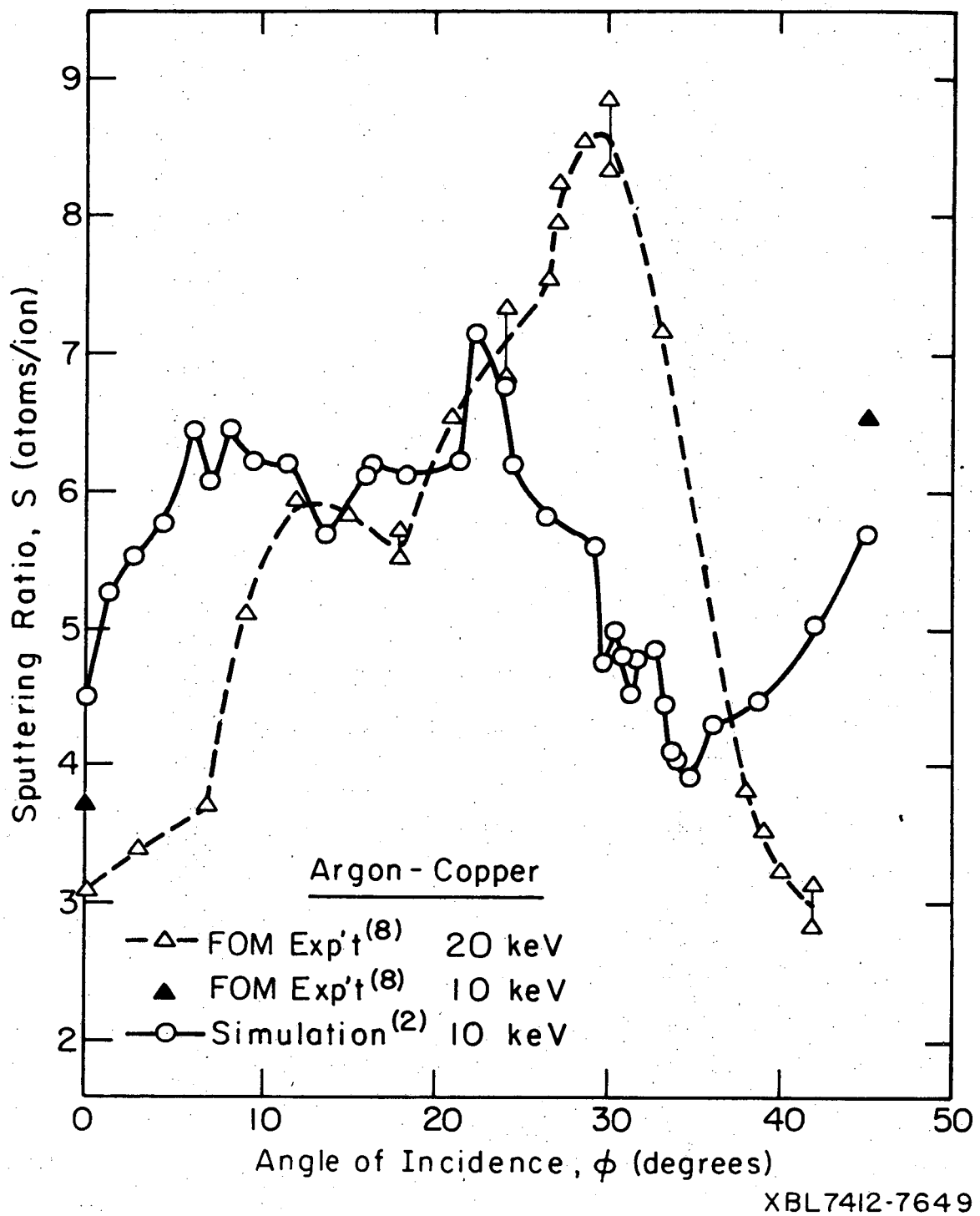

Fig. 5. Experimental and simulation sputtering ratios of Ar^+ on (100) Cu rotated about a ⟨001⟩ axis in the surface.

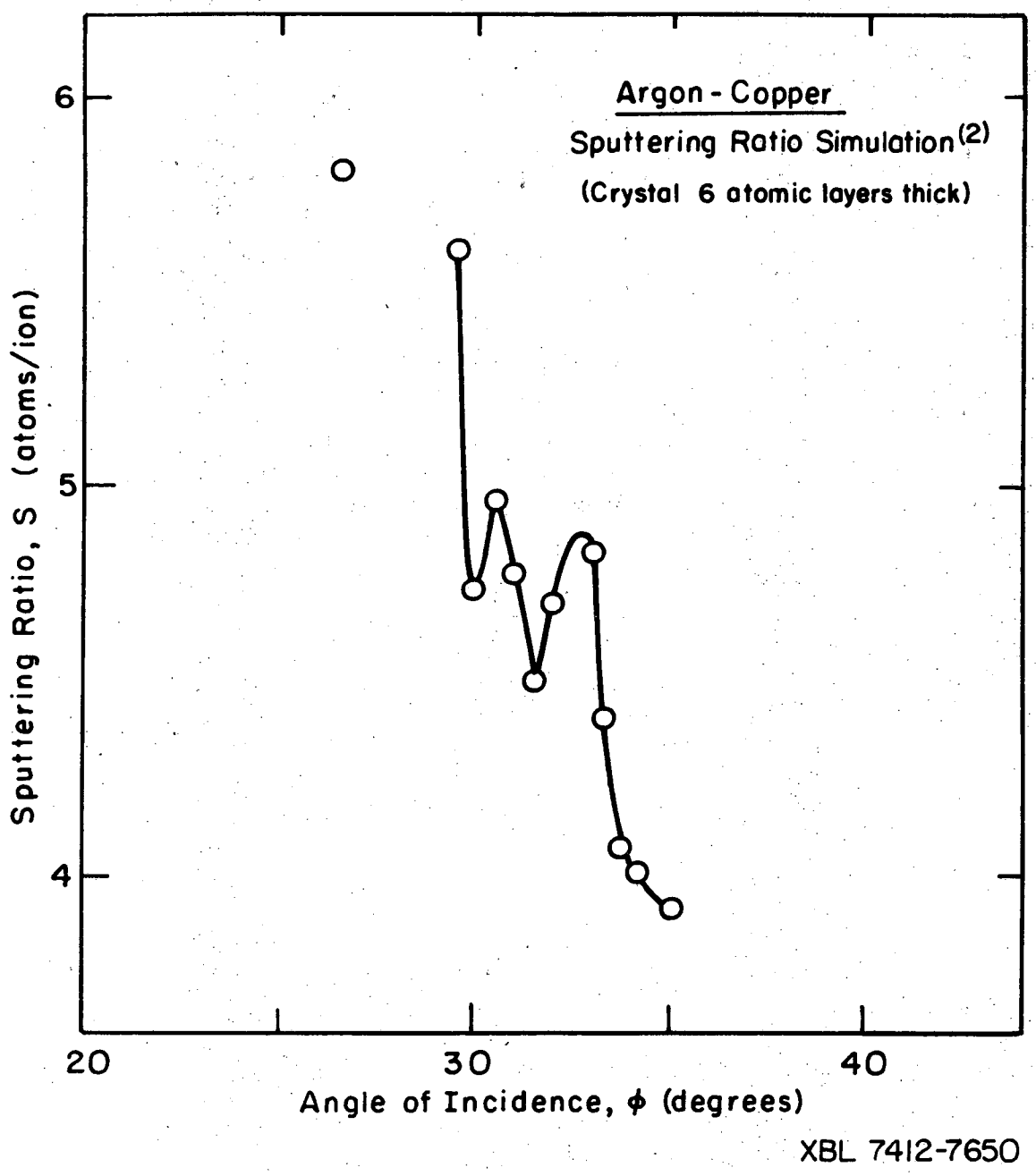

Fig. 6. Magnification of 'peak' obtained in the simulation of oblique incidence sputtering of (100) Cu by 10 keV Ar^+.

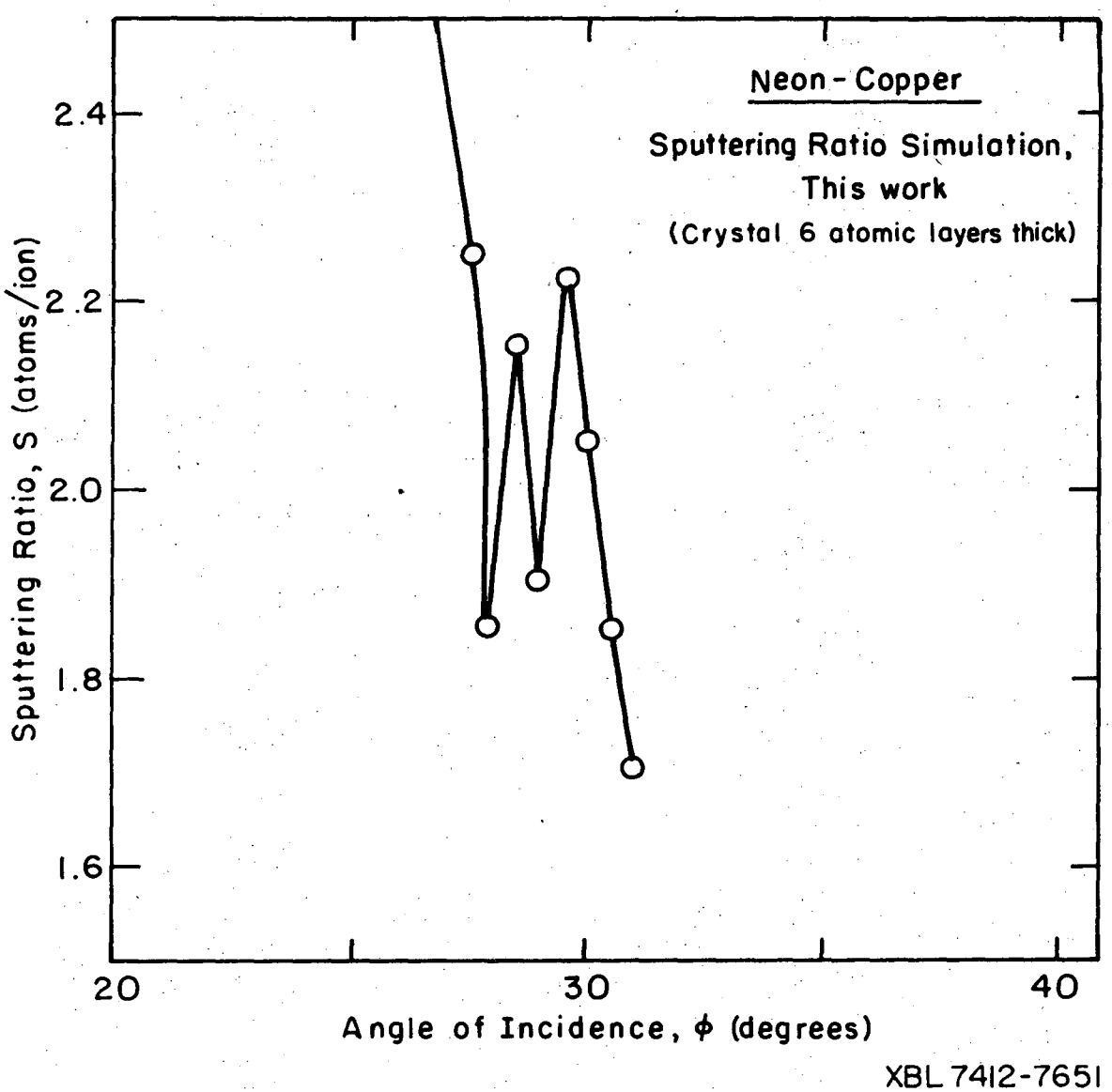

Fig. 7. Magnification of 'peak' obtained in the simulation of oblique incidence sputtering of (100) Cu by 10 keV Ne^+.

7. Conclusion

The results of the simulation match the experimental results fairly well, when corrected for the approximation of the use of only one-quarter of the true representative area for oblique incidence sputtering of monocrystalline copper by Neon.

The simulated maxima and minima near 30° and 45°, respectively, are confirmed by the simulation, but require correction for the reduced representative area for sputtering. The correction for this effect involves a shift of the simulation results to larger angles by about 5° bringing the simulation results for $S(\phi)$ into approximate agreement with experimental values.

Although the simulation points show considerable scatter a submaximum is displayed between the simulated maximum and minimum at about the same relative angle as obtained experimentally. This simulated peak is stronger for Neon-Copper sputtering than for Argon-Copper sputtering.

REFERENCES

1. J.J. Ph. Elich, H.E. Roosendaal, H.H. Kerston, D. Onderdelinden, J. Kistemaker and J.D. Elen, Radiation Effects 8, 1 (1971).
2. D.E. Harrison, Jr., W.L. Moore, Jr. and H.T. Holcombe, Radiation Effects 17, 167 (1973).
3. D.E. Harrison, Jr., Radiation Effects 40 (9), 3870 (1969).
4. D.E. Harrison, Jr., W.L. Gay and H.M. Effron, J. Math. Phys. 10 (7), 1179 (1969).
5. D.E. Harrison, Jr., N.S. Levy, J.P. Johnson, III, and H.M. Effron, J. App. Phys. 39 (8), 3742 (1968).
6. D.E. Harrison, Jr., J.P. Johnson, III, and N.S. Levy, Appl. Phys. Lit. 8 (2), 33 (1966).
7. W.L. Gay and D.E. Harrison, Jr., Phys. Rev. 135 (6A), A1780 (1964).
8. D. Onderdelinden, Thesis, University of Leiden (1968), pp. 32, 45.
9. D. Onderdelinden, F.W. Saris and P.K. Rol, Proc. of the Seventh Int. Conf. on Phen. Ion. Gases., Vol I (Beograd, 1966).
10. I.N. Evdokimov, V.A. Molchanov, Con. J. Phys. 46, 779 (1968).
11. G. Liebfried, Bestrohlungesftekte in Festkörpern (Teubner Verlagsgesltschaft, Stuttgart 1965), p. 218.
12. G. Carter and J.S. Colligon, "Ion Bombardment of Solids," American Elsevier Publishing Co., pp. (1968).
13.

LIST OF SYMBOLS

d:	Distance between neighboring atoms, a string of atoms along the ⟨110⟩ direction.
$E_f^{(110)}$:	Focusing energy in ⟨110⟩ direction (e.v.)
$E_r^{(110)}$:	Replacement energy in the ⟨110⟩ direction (e.v.)
r:	Distance between two atoms (l.u.)
V(r):	Interaction energy between two atoms a distance 'r' apart (e.v.)
P_A, P_B:	Parameters of the potential function V(r)
ΔZ:	Length over which focusing chains in the ⟨110⟩ direction are initiated by an ion incident close to the ⟨110⟩ direction.
α:	Exponent in the equation expressing the variation of the sputtering ratio, S, with the angle of incidence ϕ.
ΔZ:	Length of a chain of atoms in the ⟨110⟩ direction, over which perpendicular focusing chains in the ⟨110⟩ direction are generated by an incident ion close to the ⟨110⟩ direction.
ϕ:	Angle of incidence, w.r.t. surface normal, of an incident ion beam (degrees).
ψ:	Angle of incidence w.r.t. ⟨110⟩ axis ($\phi = -\pi/4$) Text: [Fig. (B.3-.)]

APPENDIX

The Simulation Model

The computer simulation model developed by Harrison et al.[1-6] to simulate the sputtering of mono-crystalline copper by rare gas atoms is described here.

1. General Description

The objective of this model is to simulate an ion impacting a crystal surface, to follow the motion of this ion through the crystal and also to trace the paths of those moving atoms that are created due to interactions between the ion and the lattice atoms. Any atoms ejected from the crystal surface would qualify as sputtered atoms.

It is not possible to simulate a crystal of semi-infinite proportions on the computer but a microcrystallite which is large enough to essentially contain, within itself, all the atom-atom interactions which eventually lead to sputtering, may be simulated. A rectangular parallelopiped type of microcrystallite containing about two hundred atoms is normally sufficient.

The target atoms are first positioned in the desired crystal structure so that a microcrystallite of specified size and shape is obtained. The microcrystallite is so set up that the front surface of the microcrystallite presents the desired orientation to the impacting ion.

Next, the movement of the ion through the microcrystallite is followed. Given the positions of the atoms at any instant 't', the forces between the atoms, at that instant, may be very simply calculated. Using a numerical integration procedure, the position of the atoms after a timestep 'Δt' may be estimated. By repeating the cycle of calculations the trajectory of the atoms may be followed.

The accuracy of the calculations depends on the length of the timesteps 'Δt' used in the Numerical Integration Scheme. In general, errors will increase with increasing Δt and vice-versa. Also, a more complex numerical integration scheme will give less error in the calculations, for a given 'Δt', but the computation time required will be larger.

The value of Δt must be so chosen that a certain minimum accuracy of calculations is maintained while the computation time is reasonable.

2. The Potential Function

In order to estimate the forces between atoms, the function describing the potential energy of interaction of these atoms must be available. If the potential energy of interaction of two atoms separated by a distance 'r' is given by 'V(r)', the repulsive force between these atoms is:

$$F(r) = \frac{-\,dV(r)}{dr} \qquad (2\text{-}1)$$

where F(r) is the force and the minus sign is included to show that force is repulsive.

In order to avoid the expense of wasteful computation on weak interactions, the function V(r) used in the model is 'truncated' to a 'finite range' potential. This potential may then be expressed as:

$$V(r) = V(r)-V(r_o) \quad \text{for} \quad r \leqslant r_o$$
$$= 0 \quad \text{for} \quad r > r_o \tag{2.2}$$

and the force F(r) as:

$$F(r) = \frac{-d\ V(r)}{dr} \quad \text{for} \quad r \leqslant r_o$$
$$= 0 \quad \text{for} \quad r > r_o \ . \tag{2.3}$$

A limited variety of potential functions have been investigated for the suitability of their use in the computer simulation. Functions including potential wells and attractive 'tails' have been utilized.[1]

It has been found, however, that for investigations on the nature of the sputtering phenomena, it is adequate to use short-range potentials of the Born-Mayer type:

$$V(r) = \exp\ (A+B\cdot r) \quad \text{for} \quad r \leqslant r_o$$
$$= 0 \quad \text{for} \quad r > r_o \tag{2.4}$$

r_o must be chosen to be small enough to exclude all insignificant interactions while yet being large enough to cause no considerable change in the sputtering ratios. Previous work[1-6] has shown that a choice of r_o given by:

$$r_o = r_N \tag{2.5}$$

where r_N is the nearest neighbor distance, is adequate.

Two separate potential functions need to be specified; one for target atom-target atom interactions and the other for the ion-target atom interactions.

3. Choice of Numerical Integration Procedure

The basic Newtons Law that governs the movement of the ith atom may be expressed as:

$$m_i \dot{\underset{\sim}{V}}_i = \underset{\sim}{F}_i(\underset{\sim}{r}_1, \underset{\sim}{r}_2, \ldots \underset{\sim}{r}_n) \tag{3.1}$$

where, m_i is the mass of the ith atom, $\underset{\sim}{V}_i$ is the vector velocity of the ith atom, $\underset{\sim}{F}_i$ is the total external vector force acting on the atom, and $\underset{\sim}{r}_j$ is the vector position coordinate of the jth atom (j=1,...n). Dropping the terms in the bracket and reducing the equation to one dimension for simplicity,

$$m_i \dot{V}_i = F_i \tag{3.2}$$

Also,

$$a_i = \dot{V}_i = d\, V_i/dt \tag{3.3}$$

and

$$V_i = \dot{X}_i = d\, X_i/dt\ . \tag{3.4}$$

The equations for numerical integration are developed from these simple equations. Much unpublished work[7] has shown that complicated numerical procedures allow smaller values of 'Δt' to be used but the number of computations per step is increased to such an extent that no saving in overall computation time is achieved. Hence, the available choice of numerical integration algorithms settles between two alternatives.[3]

a) The Central-Difference (C.D.) approach.

b) The Average-Force (A.F.) approach.

a) In the Central Difference approach the finite difference equivalents of Eqs. (3.2) and (3.4) are:

$$m^{-1}F_i\ [x_i(t)] \approx [V_i(t+\Delta t/2) - V_i(t-\Delta t/2)]/\Delta t \qquad (3.5)$$

and

$$V_i(t+\Delta t/2) = \dot{x}_i(t=\Delta t/2) \approx [x_i(t+\Delta t) - x_i(t)]/\Delta t \qquad (3.6)$$

(3.5) and (3.6) may be rearranged to:

$$V_i(t+\Delta t/2) = V_i(t-\Delta t/2) + F_i[x_i(t)]m^{-1}\Delta t \qquad (3.7)$$

and

$$x_i(t+\Delta t) = x_i(t) + V_i(t-\Delta t/2)\ \Delta t + F_i[x_i(t)] \cdot m^{-1} \cdot \Delta t^2 \qquad (3.8)$$

Hence, from the values of $V_i(t-\Delta t/2)$ and $x_i(t)$, $V_i(t+\Delta t/2)$ and $x_i(t+\Delta t)$ may be estimated. As may be evident, for each timestep Δt, only one computation of the forces $F_i[x_i(t)]$ is required.

One slight draw back is that velocities and positions are not obtained at the same instant of time and this leads to a few difficulties in following the process dynamically.

b) The A.F. approach is based on the Taylor series expansion of $x_i(t+\Delta t)$ about $x_i(t)$. This may be written,

$$x_i(t+\Delta t) = x_i(t) + \dot{x}_i(t)\Delta t + \ddot{x}_i(t)\Delta t^2/2 + \dddot{x}_i(t)\Delta t^3/6 + \ldots \qquad (3.9)$$

$$= x_i(t) + V_i(t)\Delta t + a_i(t)\Delta t^2/2 + \dot{a}_i(t)\ \Delta t^3/6 + \ldots \qquad (3.10)$$

If the force is relatively constant over a time interval 'Δt', $\dot{a}_i(t)$, $\ddot{a}_i(t)$ are small and it is possible to write

$$x_i(t+\Delta t) = x_i(t) + V_i(t)\Delta t + \Delta V_i(\Delta t/2) \tag{3.11}$$

where, ΔV_i is the <u>average</u> change in the velocity during Δt.

ΔV_i may then be used to define an average force $\langle F_i \rangle$:

$$\Delta V_i = \langle F_i \rangle \, m^{-1}\Delta t \tag{3.12}$$

then,

$$V_i(t+\Delta t) = V_i(t) + \langle F_i \rangle \, m^{-1}\Delta t \tag{3.13}$$

and

$$x_i(t+\Delta t) = x_i(t) + [V_i(t) + \langle F_i \rangle \, \Delta t/2m] \tag{3.14}$$

Theoretically, it should be possible to define $\langle F_i \rangle$ so that zero error is obtained in Eq. (3.13) and, conceivably, this should also lead to a small error in Eq. (3.14). This is the chief advantage of the A.F. method over the C.D. method since it is now possible to use larger values of Δt for the same error order. It must be noted that, in practice,

(i) The actual method for calculation of $\langle F_i \rangle$ will lead to some error in Eq. (3.13).

(ii) Calculation of $\langle F_i \rangle$ will necessitate evaluation of F_i (i=1...n) at least two different positions for each atom. Evaluations of F_i are time consuming. Hence, this is a disadvantage.

Another minor advantage lies in the fact that V_i and x_i are obtained at the same instant of time. This makes it easy to visualize the dynamics of the collision.

Experience gained to date has shown that the advantages of the A.F. method outweigh the disadvantages and it is superior to the C.D. method. The A.F. method was used in this work.

4. Energy Decrement

The accuracy of the numerical integration may be judged from the energy decrement

$$\Delta E = \frac{E_o - E(t)}{E(t)} \tag{4.1}$$

where, ΔE is the energy decrement, E_o is the total initial potential and kinetic energy, $E(t)$ is the total potential plus kinetic energy at any time 't'.

A poor numerical integration procedure will give a ΔE rapidly increasing in magnitude as time proceeds, while for a good integration procedure the variation of ΔE with time 't' will be slow.

5. Computation of $\langle F_i \rangle$

Given the positions x_i of the atoms at time 't', the forces $F[x_i(t)]$ may be estimated. Assuming these forces remain constant over the time interval from 't' to 't+Δt', new positions $x^*(t+\Delta t)$ may be calculated from:

$$x_i^*(t+\Delta t) = x_i(t) + V_i(t)\Delta t + F_i(x_i(t))\Delta t^2/2m \tag{5.1}$$

$x_i(t+\Delta t)$ will be a good approximation to $x_i(t+\Delta t)$, where $x_i(t+\Delta t)$ is the true position of atom 'i' at time $(t+\Delta t)$. $F_i[x_i^*(t+\Delta t)]$ may then be calculated. An estimate of F_i may then be obtained from:

$$\Delta F_i = \{F_i[x_i(t)] + F_i[x_i^*(t+\Delta t)]\}/2\cdot 0 \qquad (5.2)$$

Experience has shown that such a definition of $\langle F_i \rangle$; when utilized in (3.13) and (3.14), makes it possible to use a time interval 'Δt' at least twice that usable with the C.D. algorithm. Added to this is the fact the fact that the energy decrement, for the A.F. method, is smaller in 90% of the cases studied.

6. Choice of Δt

At the beginning of the sputtering event, the kinetic energy is localized in a few atoms. These atoms are relatively fast and hence travel longer distances in short times. Since the accuracy of the calculations is governed by the distance moved by the atoms, relative to each other, in one time step, it is desirable to have short time steps 'Δt' at this point of time in the collision cascade.

However, as the collisions proceed, the kinetic energy gets dissipated and distributed, and the atoms move slowly. The distances covered are relatively shorter and hence the errors in computation will be less. To ensure a uniform level of error at each step in the computation and also to allow the timestep to increase towards the end of the cascade (allowing more rapid convergence), the timestep 'Δt' is computed prior to each step from

$$\Delta t = (DTI)/V_{max}$$

where, V_{max} is the absolute velocity of the fastest moving atom and (DTI) is a prespecified 'time step length'. The time step length represents the maximum distance any atom may move at any particular step in the computation.

7. Designation of Sputtered Atoms

Atoms which move out of the space containing the microcrystallite from the bottom or sides are dropped from further calculations. Atoms that are ejected from the top surface are analysed separately to filter out only those atoms that have ejection energies greater than a certain minimum. Only the energy due to the velocity component perpendicular to the lattice face is considered. The 'minimum' energy represents the binding energy of copper and the atoms that filter through this barrier are the sputtered atoms.

8. Representative Areas

Finally, it must be noted that the sputtering ratios, thus obtained, are very dependent on the position on the surface at which the impacting ion enters the microcrystallite.

In order to obtain a proper value for the sputtering ratio, a set of such points must be selected and on average, of the sputtering ratios obtained over this set, must be evaluated. The set of points must be distributed over an area such that all types of possible impacts are reasonably taken into account.

The representative area for normal incidence on the (110), (100) and (111) faces are shown in Fig. 1a,b,c, respectively. Fig. 1b also indicates the representative area for oblique incidence sputtering when rotation of the crystal about the axis PT is considered. Sets of impact points must be selected from within these representative areas. In this work, two sets of points were used for the simulation.

Figure 2 indicates the twenty point set and thirty-five point set for normal-incidence sputtering on the (100) face. The sets for the (111) face are similar. In these figures, the vertex 'T' corresponds to the center of the target atoms.

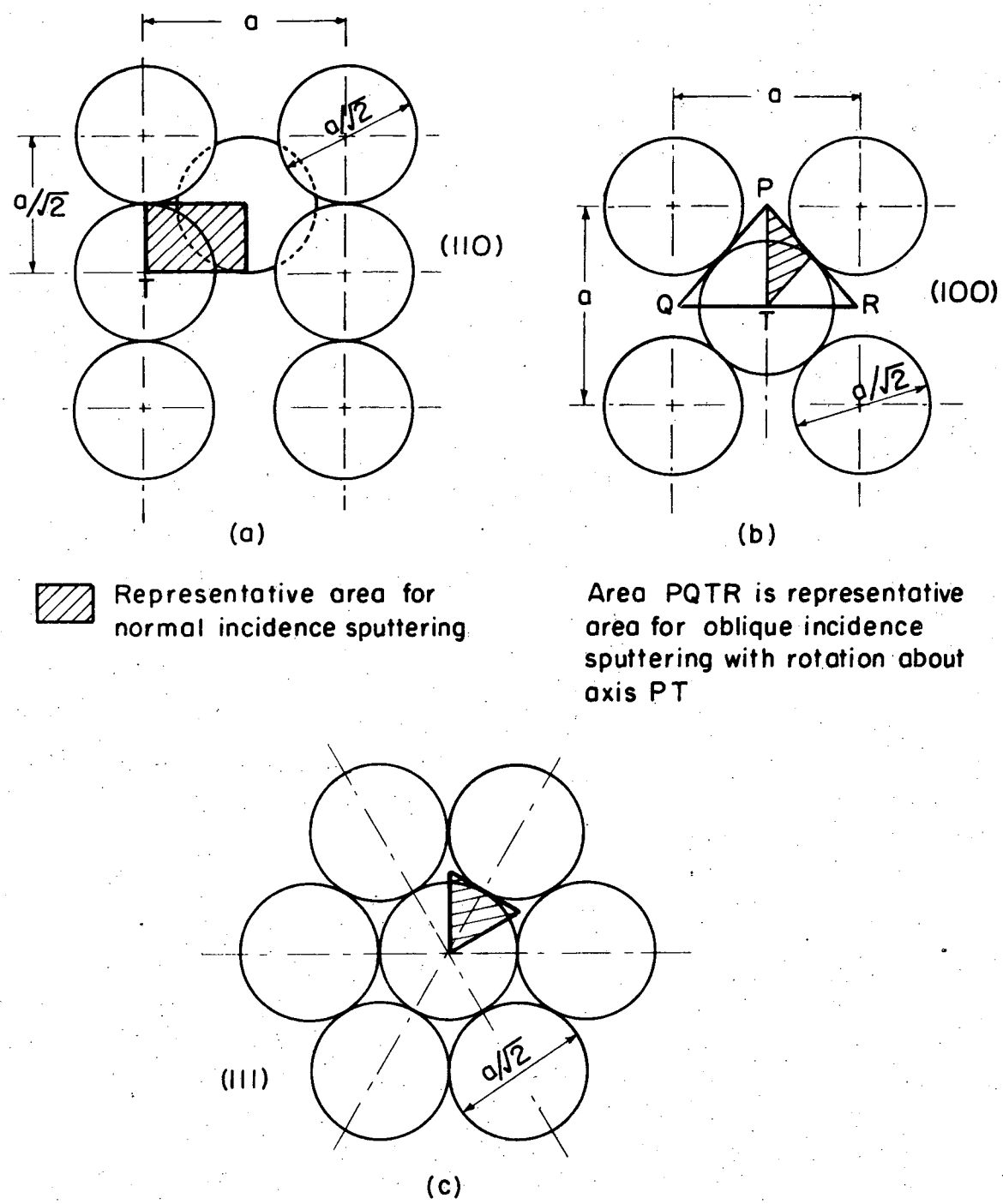

Fig. 1. The representative areas for three different crystal faces.

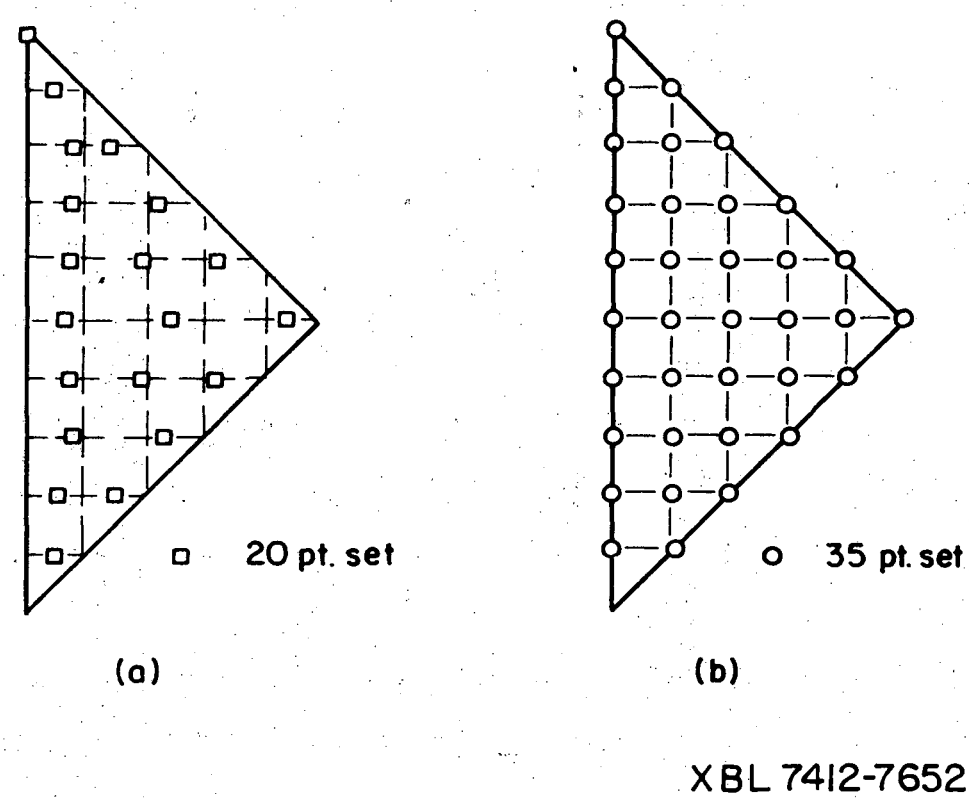

Fig. 2. The two sets of impact points used in this work.

REFERENCES

1. D.E. Harrison, Jr., W.L. Moore, Jr. and H.T. Holcombe, Radiation Effects 17, 167 (1973).
2. D.E. Harrison, Jr., J. of Appl. Phys. 40(9), 3870 (1969).
3. D.E. Harrison, Jr., W.L. Gay and H.M. Effron, J. Math. Phys. 10(7), 1179 (1969).
4. D.E. Harrison, Jr., N.S. Levy, J.P. Johnson, III, and H.M. Effron, J. of Appl. Phys. 39(8), 3742 (1968).
5. D.E. Harrison, Jr., J.P. Johnson, III, and N.S. Levy, Appl. Phys. Lett. 8(2), 33 (1966).
6. W.L. Gay and D.E. Harrison, Jr., Phys. Rev. 135(6A), A1780 (1964).
7. D.E. Harrison, Jr., (Private Communication).

LIST OF SYMBOLS

A.F.: Abbreviation for Average-Force Method, a method for numerical integration.

a: Lattice constant (=3.615Å for Cu).

a_i: Acceleration of the ith atom in one dimension.

C.D.: Abbreviation for Central-Difference Method for numerical integration.

D.T.I.: The timestep length. Maximum length that any atom may move from time 't' to 't+Δt'

E(t): Total potential and kinetic energy at time 't'.

E_o: Total initial potential and kinetic energy.

ΔE: Energy decrement.

F(r): Force function. Gives the force between two atoms that are a distance 'r' from each other.

F_i: Total external force on the ith atom (in one dimension)

$\underset{\sim}{F}_i$: Total external vector force on the ith atom.

$\langle F_i \rangle$: Average force on the ith atom from time 't' to 't+Δt'.

m_i: Mass of the ith atom.

$\underset{\sim}{r}_j$: Vector radius from origin of coordinate system to the position of the ith atom.

r_N: Nearest neighbor distance in the crystal lattice.

r_o: 'truncation' distance for a finite range potential.

t: time (sec.)

Δt: Small time increment (sec.)

$V(r)$: Potential function giving the energy of interaction of two atoms at a distance 'r' from each other.

$\underset{\sim}{V}_i$: Vector velocity of the ith atom.

$\dot{\underset{\sim}{V}}_i$ Time derivative of vector velocity V_i. Is the same as the vector acceleration of the ith atom.

V_i: Velocity of the ith atom in one dimension.

$\dot{V}_i$: Time derivative of the velocity in one dimension.

V_{max}: Absolute velocity of the fastest moving atom.

ΔV_i: Average change in the velocity of the ith atom from time 't' to '$t+\Delta t$'.

X_i: Position coordinate of the ith atom in one dimension.

$\dot{X}_i$: Time derivative of 'X_i'. Is equivalent to the velocity 'V_i' in one dimension.

X_i^*: Projected position of the ith atom at time $(t+\Delta t)$, given all conditions at time 't'.

ΔE: Energy decrement.

Δt: Small time increment (sec.).

ΔV_i: Average change in the velocity of the ith atom from time 't' to '$t+\Delta t$'.

0 0 0 0 4 2 0 1 5 4 6

LEGAL NOTICE

This report was prepared as an account of work sponsored by the United States Government. Neither the United States nor the United States Atomic Energy Commission, nor any of their employees, nor any of their contractors, subcontractors, or their employees, makes any warranty, express or implied, or assumes any legal liability or responsibility for the accuracy, completeness or usefulness of any information, apparatus, product or process disclosed, or represents that its use would not infringe privately owned rights.

TECHNICAL INFORMATION DIVISION
LAWRENCE BERKELEY LABORATORY
UNIVERSITY OF CALIFORNIA
BERKELEY, CALIFORNIA 94720